

Low-Rank Reduced Biquaternion Tensor Ring Decomposition and Tensor Completion

Hui Luo¹, Xin Liu^{2*}, Wei Liu³ and Yang Zhang⁴

¹ School of Computer Science and Engineering, Faculty of Innovation Engineering,
Macau University of Science and Technology, Macau, China

²Macau Institute of Systems Engineering, Faculty of Innovation Engineering,
Macau University of Science and Technology, Macau, China

³School of Artificial Intelligence at Sun Yat-sen University and the
Guangdong Key Laboratory of Big Data Analysis and Processing, Guangzhou, China

⁴Department of Mathematics, University of Manitoba, MB, Canada

Abstract

We define the reduced biquaternion tensor ring (RBTR) decomposition and provide a detailed exposition of the corresponding algorithm RBTR-SVD. Leveraging RBTR decomposition, we propose a novel low-rank tensor completion algorithm RBTR-TV integrating RBTR ranks with total variation (TV) regularization to optimize the process. Numerical experiments on color image and video completion tasks indicate the advantages of our method.

Keyword: Reduced biquaternion; Tensor ring decomposition; Low-rank tensor completion; Image completion; Video completion; Total variation.

AMS 2010 Subject Classification: 14N07, 15A72, 41A50.

1 Introduction

In the past decades, tensor-based learning methods are extensively used in domains like computer vision, recommender systems and signal processing [7, 16, 23]. Tensors' ability to seamlessly integrate multiple modes of information makes them particularly suited for the tasks like image reconstruction, image classification, object detection, signal reconstruction, and many other applications where traditional vector or matrix representations might fall short.

During the course of collecting, storing, or transmitting data, some information may become damaged or missing. Tensor completion arises in an effort to recover the true underlying data from these incomplete observations. The quaternion tensor completion can effectively capture the relationships among color channels and has produced outstanding results in image and video completion [1, 3, 11, 14, 19].

*Corresponding author: xiliu@must.edu.mo (Xin Liu)

Reduced biquaternions (RBs) \mathbb{H}_c is one kind of quaternion algebras [17, 21]. RBs has some notable advantages in computational efficiency and algorithmic simplicity due to its commutativity of the multiplication. For instance, the singular value decompositions (SVDs) of RB matrices are significantly more computationally efficient than ones of Hamilton quaternion matrices, requiring only a quarter of the computational efforts [19]. In [6], RBs is applied to effectively represent color images within the domain of face recognition, significantly improving the performance over traditional PCA methods. In [8], a neural network based on RBs is proposed, exhibiting commendable performance in the implementation of image denoising and image classification.

Consequently, due to its simplicity in theoretical analyses and algorithmic implementations, alongside its extensive applications in image and video processing tasks, we choose RBs for image and video representations to solve tensor completion problems in this paper.

One of the strategies for tensor completion is to minimize the rank of the tensor, thereby updating it to a lower-rank tensor that best represents the underlying structure [13], which can be presented as follows:

$$\min_{\mathcal{X}} \text{rank}(\mathcal{X}) \quad \text{s.t.} \quad P_{\Omega}(\mathcal{X}) = P_{\Omega}(\mathcal{T}), \quad (1)$$

where $\mathcal{X} \in \mathbb{H}_c^{I_1 \times I_2 \times \dots \times I_N}$ is the recovered N th-order RB tensor, $\mathcal{T} \in \mathbb{H}_c^{I_1 \times I_2 \times \dots \times I_N}$ is the observed N th-order RB tensor, and $P_{\Omega}(\cdot)$ represents the operator for projection on Ω which is the collection of indices of known entries.

To tackle this issue, we first need to choose the rank of a tensor. Typically, a tensor rank can be characterized using a variety of tensor decomposition techniques, including CP decomposition, Tucker decomposition, tensor train and tensor ring decomposition [26], etc. The tensor ring decomposition is a closed-loop structure decomposition, where each core tensor is connected in a ring, and its rank is defined by the dimensions of the core tensors in the ring. Many researches have been done on tensor ring decompositions, demonstrating its superiority in certain application scenarios compared to other methods [10, 24].

Current tensor ring decomposition methods based on real-number tensors may face limitations in capturing intrinsic channel correlations, especially in color images and videos. Leveraging the advantages of RBs, such as their ability to effectively represent interactions among multiple channels and reduce computational costs, reduced biquaternion-based tensor ring decomposition (RBTR) offers a promising solution to address these challenges. Therefore, it is essential to further establish the theoretical foundation of RBTR to enhance its applications in large-scale data storage and processing. Our main contributions are as follows:

1. We propose reduced biquaternion tensor ring decomposition, a novel tensor decomposition method employing tensor ring structures with reduced biquaternions. This method achieves lower storage costs compared to TR-SVD while maintaining comparable error levels. In image processing, it effectively preserves image quality with compressed data sizes.
2. We develop reduced biquaternion tensor ring completion, a novel tensor completion method based on reduced biquaternion image representation. By integrating RBTR rank with total variation regularization, this method achieves

superior reconstruction quality in color image and video completion compared to existing methods.

This paper is structured as follows: In Section 2, we review some definitions and properties of reduced biquaternion matrices and tensors. In Section 3, we investigate the reduced biquaternion tensor ring decomposition and propose an algorithm to solve this decomposition structure. Subsequently, in Section 4, we concentrate on the reduced biquaternion tensor completion problem, and propose a novel method rooted in the RBTR decomposition. Experimental results validating the efficacy of our approach and comparing it with other existing methods are presented in Section 5. Finally, Section 6 concludes our findings and offers insights into potential future research directions.

2 Preliminaries

In this section, we recall some definitions and properties of reduced biquaternion matrices and tensors along with the proofs of related theorems.

Reduced biquaternions (RBs) \mathbb{H}_c was introduced by Segre [22], which is an algebra over the real number field \mathbb{R} with a basis $\{1, i, j, k\}$ and has the following form:

$$\mathbb{H}_c = \{a + bi + cj + dk \mid i^2 = k^2 = -1, j^2 = 1, ij = ji = k, a, b, c, d \in \mathbb{R}\}. \quad (2)$$

Clearly, the imaginary units i, j, k also satisfy the following rules:

$$jk = kj = i, \quad ki = ik = -j.$$

Thus all elements in \mathbb{H}_c commute, that is, it is a commutative algebra. Comparing with Hamilton quaternions, beside the commutativity, another advantage of reduced biquaternions is having an orthogonal basis $\{e_1, e_2\}$ over the complex number field \mathbb{C} , which can be constructed as follows (see, e.g., [20]): for any $q \in \mathbb{H}_c$,

$$q = a + bi + cj + dk = (a + bi) + (c + di)j = q_a + q_bj = q_{c1}e_1 + q_{c2}e_2,$$

where $q_{c1} = q_a + q_b, q_{c2} = q_a - q_b, e_1$ and e_2 are defined as:

$$e_1 = \frac{1+j}{2}, \quad e_2 = \frac{1-j}{2}.$$

It is easy to see that

$$e_1e_2 = 0, \quad e_1^n = e_1^{n-1} = \dots = e_1^2 = e_1, \quad e_2^n = e_2^{n-1} = \dots = e_2^2 = e_2.$$

Moreover, the conjugate of q is $\bar{q} = a - bi + cj - dk = \bar{q}_{c1}e_1 + \bar{q}_{c2}e_2$ and its modulus is $|q| = \sqrt{a^2 + b^2 + c^2 + d^2}$.

Throughout of this paper, we will use a lowercase letter a for scalars, a bold lowercase \mathbf{a} for vectors, a bold uppercase \mathbf{A} for matrices, and calligraphic uppercase \mathcal{A} for tensors. $\Re(\cdot)$ denotes the real part of a reduced biquaternion.

For a given reduced biquaternion vector $\mathbf{q} = (q_i) \in \mathbb{H}_c^{n \times 1}$, the 2-norm is defined as $\|\mathbf{q}\|_2 = \sqrt{\sum_i |q_i|^2}$. For a given reduced biquaternion matrix $\mathbf{Q} = (q_{i,j}) \in \mathbb{H}_c^{M \times N}$, its Frobenius norm is defined as: $\|\mathbf{Q}\|_F = \sqrt{\sum_{i,j} |q_{i,j}|^2}$ and its nuclear norm is defined as $\|\mathbf{Q}\|_* = \sum_i |\sigma_i(\mathbf{Q})|$, where $\sigma_i(\mathbf{Q})$ is the i -th singular value of \mathbf{Q} . The conjugate

transpose \mathbf{Q}^H of \mathbf{Q} is defined as $\mathbf{Q}^H = (a_{i,j})^H = (\overline{a_{j,i}}) \in \mathbb{H}_c^{N \times M}$. The trace of a square RB matrix \mathbf{A} is defined in a usual way, denoted by $\text{Tr}(\mathbf{A})$.

On the other hand, we can use the orthogonal basis $\{e_1, e_2\}$ to represent a reduced biquaternion matrix $\mathbf{Q} = \mathbf{A} + \mathbf{B}i + \mathbf{C}j + \mathbf{D}k \in \mathbb{H}_c^{M \times N}$ with $\mathbf{A}, \mathbf{B}, \mathbf{C}, \mathbf{D} \in \mathbb{R}^{M \times N}$ as follows:

$$\mathbf{Q} = (\mathbf{A} + \mathbf{B}i) + (\mathbf{C} + \mathbf{D}i)j = \mathbf{Q}_a + \mathbf{Q}_b j = \mathbf{Q}_{c1} e_1 + \mathbf{Q}_{c2} e_2, \quad (3)$$

where $\mathbf{Q}_{c1}, \mathbf{Q}_{c2} \in \mathbb{C}^{M \times N}$ and $\mathbf{Q}_{c1} = \mathbf{Q}_a + \mathbf{Q}_b, \mathbf{Q}_{c2} = \mathbf{Q}_a - \mathbf{Q}_b$. By the definition of the conjugate transpose \mathbf{Q}^H , we have $\mathbf{Q}^H = \mathbf{Q}_{c1}^H e_1 + \mathbf{Q}_{c2}^H e_2$. Moreover, a complex representation of \mathbf{Q} is given by

$$\begin{bmatrix} \mathbf{Q}_{c1} & 0 \\ 0 & \mathbf{Q}_{c2} \end{bmatrix} \in \mathbb{C}^{2M \times 2N}. \quad (4)$$

A real representation of $\mathbf{Q} = \mathbf{A} + \mathbf{B}i + \mathbf{C}j + \mathbf{D}k \in \mathbb{H}_c^{M \times N}$, $\mathbf{A}, \mathbf{B}, \mathbf{C}, \mathbf{D} \in \mathbb{R}^{M \times N}$ is given by

$$\mathbf{Q}^R = \begin{bmatrix} \mathbf{A} & -\mathbf{B} & \mathbf{C} & -\mathbf{D} \\ \mathbf{B} & \mathbf{A} & \mathbf{D} & \mathbf{C} \\ \mathbf{C} & -\mathbf{D} & \mathbf{A} & -\mathbf{B} \\ \mathbf{D} & \mathbf{C} & \mathbf{B} & \mathbf{A} \end{bmatrix}.$$

Lemma 2.1. (*Reduced biquaternion singular value decomposition RBSVD*)[19]
With the notations in the formula (3), if the SVDs of \mathbf{Q}_{c1} and \mathbf{Q}_{c2} are in the following forms:

$$\mathbf{Q}_{c1} = \mathbf{U}_1 \mathbf{\Sigma}_1 \mathbf{V}_1^H, \quad \mathbf{Q}_{c2} = \mathbf{U}_2 \mathbf{\Sigma}_2 \mathbf{V}_2^H,$$

then the SVD of \mathbf{Q} is

$$\mathbf{Q} = \mathbf{U} \mathbf{\Sigma} \mathbf{V}^H, \quad (5)$$

where $\mathbf{U} = \mathbf{U}_1 e_1 + \mathbf{U}_2 e_2$, $\mathbf{\Sigma} = \mathbf{\Sigma}_1 e_1 + \mathbf{\Sigma}_2 e_2$, $\mathbf{V} = \mathbf{V}_1 e_1 + \mathbf{V}_2 e_2$.

There are several different definitions of the ranks of matrices over commutative rings. For our purpose, using above RBSVD, we define *the rank of a RB matrix \mathbf{A}* to be the number of its non-zero singular values, that is, $\text{rank}(\mathbf{A}) = \text{rank}(\mathbf{\Sigma})$. Next, we will derive some useful results about the rank of RB matrix \mathbf{A} .

Theorem 2.2. *Assume that $q = a + bi + cj + dk \neq 0 \in \mathbb{H}_c$. Then $\text{rank}(q^R) = 4$.*

Proof. For $q \in \mathbb{H}_c$, its real representation is given by

$$q^R = \begin{bmatrix} a & -b & c & -d \\ b & a & d & c \\ c & -d & a & -b \\ d & c & b & a \end{bmatrix}.$$

Now we show that each two columns of q^R are linearly independently. Support that there exists a nonzero real number k such that

$$\begin{bmatrix} a \\ b \\ c \\ d \end{bmatrix} = k \begin{bmatrix} -b \\ a \\ -d \\ c \end{bmatrix},$$

that is,

$$a = -kb, \quad b = ka, \quad c = -kd, \quad d = kc. \quad (6)$$

Thus we have $(1 + k^2)a = 0$, $(1 + k^2)c = 0$, which imply $a = 0$, $c = 0$. According to the relations in (6), we obtain $b = 0$, $d = 0$, and then $q = 0$, a contradiction to the assumption $q = a + bi + cj + dk \neq 0$. Hence, we proved the first and second column of q^R are linearly independently. Similarly, we can show that any two columns of q^R are also linearly independently. Therefore, if $q = a + bi + cj + dk \neq 0$, then $\text{rank}(q^R) = 4$. \square

Some of the following properties of the real representations are well-known (see, e.g., [5]).

Lemma 2.3. *Let $\mathbf{A}, \mathbf{B} \in \mathbb{H}_c^{M \times N}$, $\mathbf{C} \in \mathbb{H}_c^{N \times S}$, $a \in \mathbb{R}$. Then:*

- (a) $(\mathbf{A} + \mathbf{B})^R = \mathbf{A}^R + \mathbf{B}^R$, $(a\mathbf{A})^R = a\mathbf{A}^R$;
- (b) $(\mathbf{AC})^R = \mathbf{A}^R\mathbf{C}^R$;
- (c) $(\mathbf{A}^H)^R = (\mathbf{A}^R)^T$;
- (d) \mathbf{U} is unitary if and only if \mathbf{U}^R is orthogonal;
- (e) $\text{rank}(\mathbf{A}^R) = 4 \cdot \text{rank}(\mathbf{A})$;
- (f) $\text{rank}(\mathbf{AB}) \leq \min\{\text{rank}(\mathbf{A}), \text{rank}(\mathbf{B})\}$.

Proof. (a)-(c) are known in [5]. We only need to prove (d)-(f). To show (d), applying the real representation operator on the $\mathbf{U}\mathbf{U}^H = \mathbf{I}_n$ gives $\mathbf{U}^R(\mathbf{U}^H)^R = \mathbf{I}_n^R$. Using (c), we get $\mathbf{U}^R(\mathbf{U}^R)^T = \mathbf{I}_{4n}$.

To prove (e), let the SVD of $\mathbf{A} = \mathbf{U}\mathbf{\Sigma}\mathbf{V}^H$. By (b), (c) and (d), we have

$$\mathbf{A}^R = \mathbf{U}^R\mathbf{\Sigma}^R(\mathbf{V}^H)^R = \mathbf{U}^R\mathbf{\Sigma}^R(\mathbf{V}^R)^T.$$

Again, by (d), \mathbf{U}^R and $(\mathbf{V}^R)^T$ are orthogonal matrices, we obtain

$$\text{rank}(\mathbf{A}^R) = \text{rank}(\mathbf{\Sigma}^R).$$

Next, we prove $\text{rank}(\mathbf{\Sigma}^R) = 4 \cdot \text{rank}(\mathbf{\Sigma})$. Without loss of generalization and for simplicity, we assume that $\mathbf{\Sigma}$ is a 2×2 matrix. According to [19], $\mathbf{\Sigma}$ should be in the form of

$$\mathbf{\Sigma} = \begin{bmatrix} \sigma_1 & 0 \\ 0 & \sigma_2 \end{bmatrix} = \begin{bmatrix} a_1 & 0 \\ 0 & a_2 \end{bmatrix} + \begin{bmatrix} c_1 & 0 \\ 0 & c_2 \end{bmatrix} j, \quad a_1, a_2, c_1, c_2 \in \mathbb{R}.$$

Then

$$\mathbf{\Sigma}^R = \begin{bmatrix} a_1 & 0 & 0 & 0 & c_1 & 0 & 0 & 0 \\ 0 & a_2 & 0 & 0 & 0 & c_2 & 0 & 0 \\ 0 & 0 & a_1 & 0 & 0 & 0 & c_1 & 0 \\ 0 & 0 & 0 & a_2 & 0 & 0 & 0 & c_2 \\ c_1 & 0 & 0 & 0 & a_1 & 0 & 0 & 0 \\ 0 & c_2 & 0 & 0 & 0 & a_2 & 0 & 0 \\ 0 & 0 & c_1 & 0 & 0 & 0 & a_1 & 0 \\ 0 & 0 & 0 & c_2 & 0 & 0 & 0 & a_2 \end{bmatrix}.$$

Upon some arrangements of rows and columns

$$\Sigma^R \rightarrow \begin{bmatrix} a_1 & 0 & c_1 & 0 & 0 & 0 & 0 & 0 \\ 0 & a_1 & 0 & c_1 & 0 & 0 & 0 & 0 \\ c_1 & 0 & a_1 & 0 & 0 & 0 & 0 & 0 \\ 0 & c_1 & 0 & a_1 & 0 & 0 & 0 & 0 \\ 0 & 0 & 0 & 0 & a_2 & 0 & c_2 & 0 \\ 0 & 0 & 0 & 0 & 0 & a_2 & 0 & c_2 \\ 0 & 0 & 0 & 0 & c_2 & 0 & a_2 & 0 \\ 0 & 0 & 0 & 0 & 0 & c_2 & 0 & a_2 \end{bmatrix} = \begin{bmatrix} \sigma_1^R & 0 \\ 0 & \sigma_2^R \end{bmatrix},$$

where $\sigma_1 = a_1 + c_1j, \sigma_2 = a_2 + c_2j$. Obviously, if $\sigma_1 \neq 0, \sigma_2 \neq 0$, then by Theorem 2.2, we get $\text{rank}(\Sigma^R) = 8$, i.e., $\text{rank}(\Sigma^R) = 4 \cdot \text{rank}(\Sigma)$. Therefore, by the definition of rank of \mathbf{A} ,

$$\text{rank}(\mathbf{A}) = \text{rank}(\Sigma) = \frac{1}{4} \cdot \text{rank}(\Sigma^R) = \frac{1}{4} \cdot \text{rank}(\mathbf{A}^R).$$

Basing on (e), we can show (f) as follows.

By (a) and (e),

$$\text{rank}(\mathbf{AB}) = \frac{1}{4} \cdot \text{rank}((\mathbf{AB})^R) = \frac{1}{4} \cdot \text{rank}(\mathbf{A}^R \mathbf{B}^R).$$

Moreover, for the real matrices $\mathbf{A}^R, \mathbf{B}^R$,

$$\text{rank}(\mathbf{A}^R \mathbf{B}^R) \leq \min\{\text{rank}(\mathbf{A}^R), \text{rank}(\mathbf{B}^R)\} = 4 \cdot \min\{\text{rank}(\mathbf{A}), \text{rank}(\mathbf{B})\}.$$

Therefore

$$\text{rank}(\mathbf{AB}) \leq \min\{\text{rank}(\mathbf{A}), \text{rank}(\mathbf{B})\}.$$

□

Next, we verify that the norm for RB vectors has the similar properties as the norm for real number vectors. We will use these properties in next sections.

Theorem 2.4. Let $\mathbf{x}, \mathbf{y} \in \mathbb{H}_c^{n \times 1}$, where $\mathbf{x} = \mathbf{x}_0 + \mathbf{x}_1i + \mathbf{x}_2j + \mathbf{x}_3k$ and $\mathbf{y} = \mathbf{y}_0 + \mathbf{y}_1i + \mathbf{y}_2j + \mathbf{y}_3k$ with $\mathbf{x}_l, \mathbf{y}_l \in \mathbb{R}^{n \times 1} (l = 1, 2, 3, 4)$. Then

$$(a) \quad \|\mathbf{x} - \mathbf{y}\|_2^2 = \|\mathbf{x}\|_2^2 + \|\mathbf{y}\|_2^2 - 2\Re(\mathbf{x}^H \mathbf{y});$$

$$(b) \quad \Re(\mathbf{x}^H \mathbf{y}) \leq \|\mathbf{x}\|_2 \|\mathbf{y}\|_2.$$

Proof. For part (a), we have

$$\begin{aligned} \|\mathbf{x} - \mathbf{y}\|_2^2 &= \|\mathbf{x}_0 - \mathbf{y}_0\|_2^2 + \|\mathbf{x}_1 - \mathbf{y}_1\|_2^2 + \|\mathbf{x}_2 - \mathbf{y}_2\|_2^2 + \|\mathbf{x}_3 - \mathbf{y}_3\|_2^2 \\ &= \|\mathbf{x}_0\|_2^2 + \|\mathbf{y}_0\|_2^2 - 2\mathbf{x}_0^T \mathbf{y}_0 + \|\mathbf{x}_1\|_2^2 + \|\mathbf{y}_1\|_2^2 - 2\mathbf{x}_1^T \mathbf{y}_1 \\ &\quad + \|\mathbf{x}_2\|_2^2 + \|\mathbf{y}_2\|_2^2 - 2\mathbf{x}_2^T \mathbf{y}_2 + \|\mathbf{x}_3\|_2^2 + \|\mathbf{y}_3\|_2^2 - 2\mathbf{x}_3^T \mathbf{y}_3 \\ &= \|\mathbf{x}\|_2^2 + \|\mathbf{y}\|_2^2 - 2(\mathbf{x}_0^T \mathbf{y}_0 + \mathbf{x}_1^T \mathbf{y}_1 + \mathbf{x}_2^T \mathbf{y}_2 + \mathbf{x}_3^T \mathbf{y}_3), \end{aligned}$$

and

$$\begin{aligned} \Re(\mathbf{x}^H \mathbf{y}) &= \Re((\mathbf{x}_0 + \mathbf{x}_1i + \mathbf{x}_2j + \mathbf{x}_3k)^H (\mathbf{y}_0 + \mathbf{y}_1i + \mathbf{y}_2j + \mathbf{y}_3k)) \\ &= \Re((\mathbf{x}_0 - \mathbf{x}_1i + \mathbf{x}_2j - \mathbf{x}_3k)^T (\mathbf{y}_0 + \mathbf{y}_1i + \mathbf{y}_2j + \mathbf{y}_3k)) \\ &= \mathbf{x}_0^T \mathbf{y}_0 + \mathbf{x}_1^T \mathbf{y}_1 + \mathbf{x}_2^T \mathbf{y}_2 + \mathbf{x}_3^T \mathbf{y}_3. \end{aligned}$$

Thus

$$\|\mathbf{x} - \mathbf{y}\|_2^2 = \|\mathbf{x}\|_2^2 + \|\mathbf{y}\|_2^2 - 2\Re(\mathbf{x}^H \mathbf{y}),$$

which completes the proof of part (a).

For part (b), let $\mathbf{M} = \begin{bmatrix} \mathbf{x}_0 \\ \mathbf{x}_1 \\ \mathbf{x}_2 \\ \mathbf{x}_3 \end{bmatrix}$, $\mathbf{N} = \begin{bmatrix} \mathbf{y}_0 \\ \mathbf{y}_1 \\ \mathbf{y}_2 \\ \mathbf{y}_3 \end{bmatrix} \in \mathbb{R}^{4n \times 1}$. Then, applying the Cauchy-Schwarz inequality

$$|\mathbf{M}^T \mathbf{N}| \leq \|\mathbf{M}\|_2 \|\mathbf{N}\|_2,$$

we obtain

$$|\Re(\mathbf{x}^H \mathbf{y})| = |\mathbf{M}^T \mathbf{N}| \leq \|\mathbf{x}\|_2 \|\mathbf{y}\|_2.$$

□

Theorem 2.5. *Given the parameters $\beta > 0, \lambda > 0$, and let $\mathbf{x}, \mathbf{y} \in \mathbb{H}_c^{n \times 1}$. The closed-form solution to the minimization problem*

$$\min_{\mathbf{x} \in \mathbb{H}_c^{n \times 1}} f(\mathbf{x}) = \frac{\beta}{2} \|\mathbf{x} - \mathbf{y}\|_2^2 + \lambda \|\mathbf{x}\|_2$$

is given by

$$\hat{\mathbf{x}} = \max \left\{ \|\mathbf{y}\|_2 - \frac{\lambda}{\beta}, 0 \right\} \frac{\mathbf{y}}{\|\mathbf{y}\|_2}.$$

Proof. We consider two cases based on the value of $\|\mathbf{y}\|_2$ relative to $\frac{\lambda}{\beta}$:

Case 1: $\|\mathbf{y}\|_2 \leq \frac{\lambda}{\beta}$. We will prove that $\hat{\mathbf{x}} = \mathbf{0}$.

For all $\mathbf{x} \neq \mathbf{0}$, it follows from Theorem 2.4 that

$$\begin{aligned} f(\mathbf{x}) - f(\mathbf{0}) &= \frac{\beta}{2} \|\mathbf{x} - \mathbf{y}\|_2^2 + \lambda \|\mathbf{x}\|_2 - \frac{\beta}{2} \|\mathbf{y}\|_2^2 \\ &= \frac{\beta}{2} (\|\mathbf{x}\|_2^2 + \|\mathbf{y}\|_2^2 - 2\Re(\mathbf{x}^H \mathbf{y})) + \lambda \|\mathbf{x}\|_2 - \frac{\beta}{2} \|\mathbf{y}\|_2^2 \\ &= \frac{\beta}{2} \|\mathbf{x}\|_2^2 - \beta \Re(\mathbf{x}^H \mathbf{y}) + \lambda \|\mathbf{x}\|_2. \end{aligned}$$

As proven in Theorem 2.4 part (b), we have $|\Re(\mathbf{x}^H \mathbf{y})| \leq \|\mathbf{x}\|_2 \|\mathbf{y}\|_2$, and thus

$$\begin{aligned} f(\mathbf{x}) - f(\mathbf{0}) &\geq \frac{\beta}{2} \|\mathbf{x}\|_2^2 - \beta \|\mathbf{x}\|_2 \|\mathbf{y}\|_2 + \lambda \|\mathbf{x}\|_2 \\ &\geq \frac{\beta}{2} \|\mathbf{x}\|_2^2 + \|\mathbf{x}\|_2 (\lambda - \beta \|\mathbf{y}\|_2). \end{aligned}$$

Note that $\lambda - \beta \|\mathbf{y}\|_2 \geq 0$, and thus $f(\mathbf{x}) - f(\mathbf{0}) > 0$, which implies that $\hat{\mathbf{x}} = \mathbf{0}$.

Case 2: $\|\mathbf{y}\|_2 > \frac{\lambda}{\beta}$. We will find the $\hat{\mathbf{x}}$ which minimizes $f(\mathbf{x})$.

By setting the gradient of $f(\mathbf{x})$ to be zero, we have

$$\beta(\mathbf{x} - \mathbf{y}) + \lambda \frac{\mathbf{x}}{\|\mathbf{x}\|_2} = 0.$$

Solving for \mathbf{x} yields

$$\mathbf{x} \left(\beta + \frac{\lambda}{\|\mathbf{x}\|_2} \right) - \beta \mathbf{y} = 0. \quad (7)$$

Now, taking the 2-norm of both sides gives

$$\|\mathbf{x}\|_2 \left(\beta + \frac{\lambda}{\|\mathbf{x}\|_2} \right) - \beta \|\mathbf{y}\|_2 = 0,$$

and thus

$$\|\mathbf{x}\|_2 = \|\mathbf{y}\|_2 - \frac{\lambda}{\beta}. \quad (8)$$

Substituting (8) into (7), we obtain

$$\mathbf{x} \left(\beta + \frac{\lambda}{\|\mathbf{y}\|_2 - \frac{\lambda}{\beta}} \right) - \beta \mathbf{y} = 0,$$

from which we have

$$\hat{\mathbf{x}} = \frac{\|\mathbf{y}\|_2 - \frac{\lambda}{\beta}}{\|\mathbf{y}\|_2} \mathbf{y}.$$

□

3 Reduced biquaternion tensor decomposition

First, we define the reduced biquaternion tensor ring decomposition, extending from the real-valued framework [26].

Definition 3.1. (Reduced Biquaternion Tensor Ring (RBTR) Decomposition)

Let $\mathcal{T} \in \mathbb{H}_c^{I_1 \times I_2 \times \dots \times I_N}$. The reduced biquaternion tensor ring (RBTR) decomposition is to break down \mathcal{T} into a series of latent tensors $\mathcal{Z}_k \in \mathbb{H}_c^{r_k \times I_k \times r_{k+1}}$ for $k = 1, 2, \dots, N$. Each entry of \mathcal{T} is defined through:

$$\mathcal{T}(i_1, i_2, \dots, i_N) = \text{Tr}\{\mathbf{Z}_1(i_1)\mathbf{Z}_2(i_2) \cdots \mathbf{Z}_N(i_N)\},$$

where $\mathbf{Z}_k(i_k) \in \mathbb{H}_c^{r_k \times r_{k+1}}$ indicates the i_k -th lateral slice of the latent tensor \mathcal{Z}_k , and $r_{N+1} = r_1$. $\mathbf{r} = [r_1, r_2, \dots, r_N]$ is a vector called *RBTR rank* of \mathcal{T} .

For simplicity's sake, we refer to the RBTR decomposition as $\mathcal{T} = \mathfrak{RBTR}(\mathcal{Z}_1, \mathcal{Z}_2, \dots, \mathcal{Z}_N)$.

Because the reduced biquaternions satisfy multiplicative commutativity, the definition and related proofs are simpler than Hamilton quaternions, like the property of Invariance of Circular Dimensional Permutation in Theorem 3.2.

Theorem 3.2. (Invariance of Circular Dimensional Permutation)

Let $\mathcal{T} \in \mathbb{H}_c^{I_1 \times I_2 \times \dots \times I_N}$ be a RB tensor with a RBTR format $\mathfrak{RBTR}(\mathcal{Z}_1, \mathcal{Z}_2, \dots, \mathcal{Z}_N)$. If we define $\overleftarrow{\mathcal{T}}^k \in \mathbb{H}_c^{I_{k+1} \times I_{k+2} \times \dots \times I_N \times I_1 \times I_2 \times \dots \times I_k}$ as moving the dimension of \mathcal{T} circularly by k steps, then we have $\overleftarrow{\mathcal{T}}^k = \mathfrak{RBTR}(\mathcal{Z}_{k+1}, \dots, \mathcal{Z}_N, \mathcal{Z}_1, \dots, \mathcal{Z}_k)$.

Proof. Note that \mathbb{H}_c is a commutative ring. For any RB matrices $\mathbf{P} = (p_{ij}) \in \mathbb{H}_c^{M \times N}$, $\mathbf{Q} = (q_{ij}) \in \mathbb{H}_c^{N \times M}$, we have the following same trace property as real matrices.

$$\text{Tr}(\mathbf{PQ}) = \sum_{i=1}^M \sum_{j=1}^N p_{ij} q_{ji} = \sum_{j=1}^N \sum_{i=1}^M q_{ji} p_{ij} = \text{Tr}(\mathbf{QP}).$$

Clearly, this property is also true for the product of multiple RB matrices. Therefore, we can easily prove the following process

$$\begin{aligned} & \overleftarrow{\mathcal{T}}^k(i_{k+1}, \dots, i_N, i_1, \dots, i_k) \\ &= \mathcal{T}(i_1, i_2, \dots, i_N) \\ &= \text{Tr}\{\mathbf{Z}_1(i_1) \cdots \mathbf{Z}_k(i_k) \mathbf{Z}_{k+1}(i_{k+1}) \cdots \mathbf{Z}_N(i_N)\} \\ &= \text{Tr}\{\mathbf{Z}_{k+1}(i_{k+1}) \cdots \mathbf{Z}_N(i_N) \mathbf{Z}_1(i_1) \cdots \mathbf{Z}_k(i_k)\}. \end{aligned}$$

The above proof demonstrates that moving the dimension of \mathcal{T} circularly by k steps retains the RBTR format and $\overleftarrow{\mathcal{T}}^k = \mathfrak{I}\mathfrak{R}(\mathcal{Z}_{k+1}, \dots, \mathcal{Z}_N, \mathcal{Z}_1, \dots, \mathcal{Z}_k)$. \square

Next, we merge the cores of $\mathcal{T} = \mathfrak{I}\mathfrak{R}(\mathcal{Z}_1, \mathcal{Z}_2, \dots, \mathcal{Z}_N) \in \mathbb{H}_c^{I_1 \times I_2 \times \dots \times I_N}$ in the following two ways. The new cores are called the *RB subchain tensors*.

The first way is to merge the first k cores $\mathcal{Z}_1 \dots \mathcal{Z}_k$ into a new core $\mathcal{Z}^{\leq k} \in \mathbb{H}_c^{r_1 \times \prod_{j=1}^k I_j \times r_{k+1}}$ whose lateral slice matrices are described as:

$$\mathbf{Z}^{\leq k}(:, \overline{i_1 \dots i_k}, :) = \prod_{j=1}^k \mathbf{Z}_j(i_j),$$

where $\overline{i_1 \dots i_k} = i_1 + (i_2 - 1)I_1 + (i_3 - 1)I_1 I_2 + \dots + (i_k - 1) \prod_{j=1}^{k-1} I_j$.

The second way is, in a similar way, to merge the last $N - k$ cores $\mathcal{Z}_{k+1} \dots \mathcal{Z}_N$ into a new core $\mathcal{Z}^{> k} \in \mathbb{H}_c^{r_{k+1} \times \prod_{j=k+1}^N I_j \times r_1}$, whose lateral slice matrices are described as

$$\mathbf{Z}^{> k}(:, \overline{i_{k+1} \dots i_N}, :) = \prod_{j=k+1}^N \mathbf{Z}_j(i_j).$$

where $\overline{i_{k+1} \dots i_N} = i_{k+1} + (i_{k+2} - 1)I_{k+1} + (i_{k+3} - 1)I_{k+1} I_{k+2} + \dots + (i_N - 1) \prod_{j=1}^{N-1} I_j$.

In the rest of this paper, we will use the following three common unfolding methods for reduced biquaternion tensors, which are extended from those for real-valued tensors [16]. As usual, we will use three kinds of brackets for these three unfolding methods like $\mathbf{T}_{(k)}$, $\mathbf{T}_{[k]}$ and $\mathbf{T}_{\langle k \rangle}$.

Classical Mode- k Unfolding: For $\mathcal{T} \in \mathbb{H}_c^{I_1 \times I_2 \times \dots \times I_N}$, let $\mathbf{T}_{(k)} \in \mathbb{H}_c^{I_k \times \prod_{l \neq k} I_l}$ be the classical mode- k unfolding of \mathcal{T} . The tensor element indexed by (i_1, i_2, \dots, i_N) of \mathcal{T} maps to the matrix element at position (i_k, j) -th of $\mathbf{T}_{(k)}$, i.e.,

$$\mathcal{T}(i_1, i_2, \dots, i_N) = \mathbf{T}_{(k)}(i_k, j),$$

where $j = i_1 + (i_2 - 1)I_1 + \dots + (i_{k-1} - 1) \prod_{l=1}^{k-2} I_l + (i_{k+2} - 1) \prod_{l=1, l \neq k}^{k+1} I_l + \dots + (i_N - 1) \prod_{l=1, l \neq k}^{N-1} I_l$.

Mode- k Unfolding: For $\mathcal{T} \in \mathbb{H}_c^{I_1 \times I_2 \times \dots \times I_N}$, let $\mathbf{T}_{[k]} \in \mathbb{H}_c^{I_k \times \prod_{l \neq k} I_l}$ be the mode- k unfolding of \mathcal{T} . The tensor element indexed by (i_1, i_2, \dots, i_N) of \mathcal{T} maps to the matrix element at position (i_k, j) -th of $\mathbf{T}_{[k]}$, i.e.,

$$\mathcal{T}(i_1, i_2, \dots, i_N) = \mathbf{T}_{[k]}(i_k, j),$$

where $j = i_{k+1} + (i_{k+2} - 1)I_{k+1} + \dots + (i_N - 1) \prod_{l=k+1}^{N-1} I_l + \dots + (i_{k-1} - 1) \prod_{l=k+1}^{k-2} I_l$.

k -mode Unfolding: For $\mathcal{T} \in \mathbb{H}_c^{I_1 \times I_2 \times \dots \times I_N}$, let $\mathbf{T}_{\langle k \rangle} \in \mathbb{H}_c^{\prod_{l=1}^k I_l \times \prod_{l=k+1}^N I_l}$ be the k -mode unfolding of \mathcal{T} . The tensor element indexed by (i_1, i_2, \dots, i_N) of \mathcal{T} maps to the matrix element at position (i, j) -th of $\mathbf{T}_{\langle k \rangle}$, i.e.,

$$\mathcal{T}(i_1, i_2, \dots, i_N) = \mathbf{T}_{\langle k \rangle}(i, j),$$

where $i = i_1 + (i_2 - 1)I_1 + \dots + (i_k - 1) \prod_{l=1}^{k-1} I_l$, $j = i_{k+1} + (i_{k+2} - 1)I_{k+1} + \dots + (i_N - 1) \prod_{l=k+1}^{N-1} I_l$.

The three unfolding methods have the following relation in term of subchain tensors.

Theorem 3.3. *Let $\mathcal{T} = \mathfrak{TA}(\mathcal{Z}_1, \mathcal{Z}_2, \dots, \mathcal{Z}_N) \in \mathbb{H}_c^{I_1 \times I_2 \times \dots \times I_N}$ represent a RB tensor structured in RBTR format. Then its k -mode unfolding $\mathbf{T}_{\langle k \rangle}$ can be decomposed by using (classical) mode- k unfoldings of RB subchain tensors, that is,*

$$\mathbf{T}_{\langle k \rangle} = \mathbf{Z}_{(2)}^{\leq k} (\mathbf{Z}_{[2]}^{> k})^T. \quad (9)$$

Proof. By the definition of $\mathbf{T}_{\langle k \rangle}$,

$$\begin{aligned} \mathbf{T}_{\langle k \rangle}(i, j) &= \mathcal{T}(i_1, i_2, \dots, i_N) \\ &= \text{Tr} \{ \mathbf{Z}_1(i_1) \mathbf{Z}_2(i_2) \cdots \mathbf{Z}_N(i_N) \} \\ &= \text{Tr} \left\{ \prod_{j=1}^k \mathbf{Z}_j(i_j) \prod_{j=k+1}^N \mathbf{Z}_j(i_j) \right\}. \end{aligned} \quad (10)$$

Recall that the vector operator $\text{Vec}(\cdot)$ is the column vector obtained by stacking the columns of the matrix in order. By $\text{Tr}(\mathbf{AB}) = (\text{Vec}(\mathbf{A}))^\top \text{Vec}(\mathbf{B}^\top)$, (10) becomes

$$\begin{aligned} \mathbf{T}_{\langle k \rangle}(i, j) &= \left(\text{Vec} \left(\prod_{j=1}^k \mathbf{Z}_j(i_j) \right) \right)^\top \text{Vec} \left(\prod_{j=N}^{k+1} \mathbf{Z}_j^\top(i_j) \right) \\ &= \sum_{p=1}^{r_{1r_{k+1}}} \mathbf{Z}_{(2)}^{\leq k}(i, p) \left(\mathbf{Z}_{[2]}^{> k} \right)^\top(p, j), \end{aligned}$$

where $i = \overline{i_1 i_2 \dots i_k}$ and $j = \overline{i_{k+1} i_{k+2} \dots i_N}$. From the formula of $\mathbf{T}_{\langle k \rangle}(i, j)$, we have

$$\mathbf{T}_{\langle k \rangle} = \mathbf{Z}_{(2)}^{\leq k} (\mathbf{Z}_{[2]}^{> k})^\top.$$

□

Initially, we utilize the truncated SVD technique to extract the principal characteristics of the tensor's 1-mode unfolding matrix $\mathbf{T}_{\langle 1 \rangle} \in \mathbb{H}_c^{I_1 \times \prod_{l=2}^N I_l}$. First, a threshold

$\delta_1 = \sqrt{2}\epsilon \frac{\|\mathcal{T}\|_F}{\sqrt{N}}$ is set to determine the rank of the approximation, as described in [26]. In this context, ϵ is the predefined tolerance level. Consequently, $\mathbf{T}_{\langle 1 \rangle}$ can be approximated as a low-rank matrix by retaining only the singular values that exceed the threshold δ_1 :

$$\mathbf{T}_{\langle 1 \rangle} = \mathbf{U}_1 \mathbf{\Sigma}_1 \mathbf{V}_1^H + \mathbf{E}_1, \quad (11)$$

where $\mathbf{U}_1 \in \mathbb{H}_c^{I_1 \times r_1 r_2}$ and $\mathbf{\Sigma}_1 \in \mathbb{H}_c^{r_1 r_2 \times r_1 r_2}$ and $\mathbf{V}_1^H \in \mathbb{H}_c^{r_1 r_2 \times \prod_{l=2}^N I_l}$.

By Theorem 3.3, $\mathbf{T}_{\langle 1 \rangle}$ can be rewritten as

$$\mathbf{T}_{\langle 1 \rangle} = \mathbf{Z}_{(2)}^{\leq 1} (\mathbf{Z}_{[2]}^{\geq 1})^\top.$$

Consider that $\mathbf{Z}_{(2)}^{\leq 1}$ is equivalent to \mathbf{U}_1 and $(\mathbf{Z}_{[2]}^{\geq 1})^\top$ corresponds to $\mathbf{\Sigma}_1 \mathbf{V}_1^H$. Using these, the primary core tensor \mathcal{Z}_1 of size $r_1 \times I_1 \times r_2$ is derived by appropriately reorganizing and switching the elements of \mathbf{U}_1 . Meanwhile, $\mathcal{Z}^{\geq 1}$ of size $r_2 \times \prod_{j=2}^N I_j \times r_1$ is derived by appropriately reorganizing and switching the elements of $\mathbf{\Sigma}_1 \mathbf{V}_1^H$. We can reshape $\mathcal{Z}^{\geq 1}$ into matrix $\mathbf{Z}^{\geq 1}$ of size $r_2 I_2 \times \prod_{j=3}^N I_j r_1$, and continue to apply truncated SVD by using $\delta_2 = \epsilon \frac{\|\mathcal{T}\|_F}{\sqrt{N}}$ on it:

$$\mathbf{Z}^{\geq 1} = \mathbf{U}_2 \mathbf{\Sigma}_2 \mathbf{V}_2^H + \mathbf{E}_2,$$

where $\mathbf{U}_2 \in \mathbb{H}_c^{r_2 I_2 \times r_3}$, $\mathbf{\Sigma}_2 \in \mathbb{H}_c^{r_3 \times r_3}$ and $\mathbf{V}_2^H \in \mathbb{H}_c^{r_3 \times \prod_{j=3}^N I_j r_1}$. Similarly, the second core tensor \mathcal{Z}_2 of size $r_2 \times I_2 \times r_3$ is derived by appropriately reorganizing and switching the elements of \mathbf{U}_2 . Following the same method, we can get the remaining cores \mathcal{Z}_k by setting $\delta_k = \epsilon \frac{\|\mathcal{T}\|_F}{\sqrt{N}}$, for $k > 1$.

In the following, **Algorithm 1** specifies the RBTR-SVD algorithm's detailed process.

Finally, we validate the effectiveness of RBTR-SVD by comparing storage costs, compression ratios, PSNR, and RSE under various degrees of relative errors. For our analysis, we select ten color images¹ with the size of $256 \times 256 \times 3$. Both of RBTR-SVD and TR-SVD are applied to these images and the comparative results are presented in Table 1.

The storage cost is defined as $\sum_{k=1}^K N_k$, where N_k is the number of elements in the k -th core tensor. The compression ratio is defined as $\frac{N}{S}$, where N is the total number of elements in the original tensor, and S is the storage cost which equals the sum of the elements in the core tensors.

The relative error RSE measures the difference between the original tensor \mathcal{X} and the recovered tensor $\hat{\mathcal{X}}$, which is

$$\text{RSE} = \frac{\|\hat{\mathcal{X}} - \mathcal{X}\|_F}{\|\mathcal{X}\|_F}. \quad (12)$$

Define

$$\text{PSNR} = 10 \log_{10} \left(\frac{\max^2}{\|\hat{\mathcal{X}} - \mathcal{X}\|_F / N} \right), \quad (13)$$

where \max equals the original image data's maximum pixel value, and N represents the total number of elements in the tensor.

¹<https://sipi.usc.edu/database/>

Algorithm 1 RBTR-SVD

Input: A RB tensor $\mathcal{T} \in \mathbb{H}_c^{I_1 \times I_2 \times \dots \times I_N}$ and the tolerance level ϵ .

Output: Cores \mathcal{Z}_k ($k = 1, \dots, N$) and the RBTR ranks

- 1: Set the truncation threshold: for $k = 1$, $\delta_1 = \sqrt{2}\epsilon \frac{\|\mathcal{T}\|_F}{\sqrt{N}}$, and for $k > 1$, $\delta_k = \epsilon \frac{\|\mathcal{T}\|_F}{\sqrt{N}}$.
- 2: Select the initial mode and apply a low-rank approximation to $\mathbf{T}_{\langle 1 \rangle}$ by (11) with the threshold δ_1
- 3: Determine ranks r_1 and r_2 :

$$\min_{r_1, r_2} \|r_1 - r_2\| \quad \text{subject to} \quad r_1 r_2 = \text{rank}_{\delta_1}(\mathbf{T}_{\langle 1 \rangle})$$

- 4: Compute the first core tensor:

$$\mathcal{Z}_1 = \text{permute}(\text{reshape}(\mathbf{U}_1, [I_1, r_1, r_2]), [2, 1, 3])$$

- 5: Derive another core tensor $\mathcal{Z}^{>1}$:

$$\mathcal{Z}^{>1} = \text{permute} \left(\text{reshape} \left(\Sigma_1 \mathbf{V}_1^H, [r_1, r_2, \prod_{j=2}^N I_j] \right), [2, 3, 1] \right)$$

- 6: **for** $k = 2$ to $N - 1$ **do**

- 7: $\mathcal{Z}^{>k-1} = \text{reshape} \left(\mathcal{Z}^{>k-1}, [r_k I_k, \prod_{j=k+1}^N I_j r_1] \right)$

- 8: $\mathcal{Z}^{>k-1} = \mathbf{U}_k \Sigma_k \mathbf{V}_k^H + \mathbf{E}_k$

- 9: $r_{k+1} = \text{rank}_{\delta_k}(\mathcal{Z}^{>k-1})$

- 10: $\dot{\mathcal{Z}}_k = \text{reshape}(\mathbf{U}_k, [r_k, I_k, r_{k+1}])$

- 11: $\mathcal{Z}^{>k} = \text{reshape} \left(\Sigma_k \mathbf{V}_k^H, [r_{k+1}, \prod_{j=k+1}^N I_j, r_1] \right)$

- 12: **end for**
-

Table 1 shows that, in most images, RBTR-SVD achieves higher PSNR and lower RSE compared to TR-SVD. Additionally, as the relative error level increases, the differences in PSNR and RSE between the two methods tend to decrease. However, RBTR-SVD offers a substantial reduction in storage cost at the same relative error level. Experimental results demonstrate that reduced biquaternion tensor ring decomposition is an effective representation method, reducing data size efficiently while retaining substantial information.

4 Reduced biquaternion tensor completion

As mentioned in Section 1, the low-rank reduced biquaternion tensor completion (LRRBTC) problem can be modeled as

$$\min_{\mathcal{X}} \text{rank}(\mathcal{X}), \quad s.t. \quad P_{\Omega}(\mathcal{X}) = P_{\Omega}(\mathcal{T}). \quad (14)$$

We first define $\text{rank}(\mathcal{X})$ through the RBTR decomposition. We will adopt the idea in [25] to minimize the tensor circular unfolding rank as an alternative to the tensor rank.

Relative Error	Image	TR-SVD			RBTR-SVD		
		RSE	PSNR	Storage Cost	RSE	PSNR	Storage Cost
0.005	Airplane	2.91e-03	53.39	260784 (0.75)	1.96e-03	56.82	96676 (2.03)
	Peppers	2.37e-03	58.40	296748 (0.66)	1.60e-03	61.82	98576 (1.99)
	Baboon	2.13e-03	58.75	302385 (0.65)	2.06e-14	279.07	100496 (1.96)
	Female	1.69e-03	66.33	301737 (0.65)	1.13e-14	289.85	100496 (1.96)
	House1	3.27e-03	54.32	266577 (0.74)	2.21e-03	57.72	97320 (2.02)
	Tree	2.45e-03	57.41	295544 (0.67)	1.70e-03	60.58	99216 (1.98)
	Butterfly	2.95e-03	56.31	263236 (0.75)	1.91e-03	60.09	97936 (2.01)
	House2	3.08e-03	54.04	241873 (0.81)	1.72e-03	59.09	98576 (1.99)
	Baby	3.31e-03	53.63	205937 (0.95)	3.23e-03	54.04	91812 (2.14)
Bird	3.12e-03	59.20	238109 (0.83)	3.02e-03	59.49	89976 (2.19)	
0.015	Airplane	1.05e-02	42.29	114105 (1.72)	8.94e-03	43.64	81264 (2.42)
	Peppers	8.61e-03	47.20	237677 (0.83)	8.23e-03	47.59	88224 (2.23)
	Baboon	8.52e-03	46.72	284832 (0.69)	5.16e-03	51.08	98576 (1.99)
	Female	7.80e-03	53.07	319600 (0.62)	6.63e-03	54.48	97320 (2.02)
	House1	9.64e-03	44.94	209356 (0.94)	9.05e-03	45.48	78544 (2.50)
	Tree	1.03e-02	44.92	215125 (0.91)	8.67e-03	46.42	90668 (2.17)
	Butterfly	9.82e-03	45.87	167912 (1.17)	9.13e-03	46.50	89392 (2.20)
	House2	8.75e-03	44.97	214032 (0.92)	8.39e-03	45.35	87608 (2.24)
	Baby	1.04e-02	43.87	117613 (1.67)	1.01e-02	44.09	68304 (2.88)
Bird	9.98e-03	49.11	166137 (1.18)	9.27e-03	49.75	70504 (2.79)	
0.025	Airplane	1.80e-02	37.42	115384 (1.70)	1.74e-02	37.84	65704 (2.99)
	Peppers	1.66e-02	41.51	210600 (0.93)	1.45e-02	42.65	77320 (2.54)
	Baboon	1.62e-02	41.13	249149 (0.79)	1.29e-02	43.11	94792 (2.07)
	Female	1.43e-02	47.79	262504 (0.75)	1.41e-02	47.95	91216 (2.17)
	House1	1.89e-02	39.11	141368 (1.41)	1.74e-02	39.79	59176 (3.32)
	Tree	1.50e-02	41.64	199016 (0.99)	1.49e-02	41.74	81324 (2.42)
	Butterfly	1.70e-02	41.08	125729 (1.56)	1.61e-02	41.58	80528 (2.44)
	House2	1.82e-02	38.64	127381 (1.54)	1.49e-02	40.34	75716 (2.60)
	Baby	1.96e-02	38.42	81233 (2.42)	1.94e-02	38.45	50376 (3.90)
Bird	1.68e-02	44.58	148500 (1.32)	1.87e-02	43.65	55884 (3.52)	
0.05	Airplane	3.95e-02	30.73	58146 (3.38)	3.58e-02	31.60	41556 (4.73)
	Peppers	3.45e-02	35.15	131364 (1.50)	3.20e-02	35.81	53024 (3.71)
	Baboon	3.43e-02	34.61	193380 (1.02)	2.81e-02	36.37	84660 (2.32)
	Female	3.95e-02	38.97	144033 (1.37)	3.42e-02	40.23	71356 (2.76)
	House1	4.15e-02	32.26	50718 (3.88)	3.74e-02	33.17	26532 (7.41)
	Tree	3.40e-02	34.55	112576 (1.75)	3.25e-02	34.94	58760 (3.35)
	Butterfly	3.37e-02	35.17	96984 (2.03)	3.29e-02	35.37	60880 (3.23)
	House2	3.91e-02	31.98	68053 (2.89)	3.70e-02	32.46	48208 (4.08)
	Baby	3.57e-02	31.98	52108 (3.77)	4.09e-02	31.98	24072 (8.17)
Bird	3.34e-02	38.42	91864 (2.14)	3.33e-02	38.64	35344 (5.56)	

Table 1: RSE, PSNR, Storage Costs, and Compression Ratios (in parentheses) of the algorithms

Definition 4.1. (Reduced Biquaternion Tensor Circular Unfolding)

Let $\mathcal{X} \in \mathbb{H}_c^{I_1 \times I_2 \times \dots \times I_N}$. Its circular unfolding $\mathbf{X}_{\langle k, d \rangle}$ is defined as:

$$\mathbf{X}_{\langle k, d \rangle}(\overline{i_m i_{m+1} \dots i_k}, \overline{i_{k+1} \dots i_{m-1}}) = \mathcal{X}(i_1, i_2, \dots, i_N),$$

where

$$m = \begin{cases} k - d + 1, & \text{if } d \leq k; \\ k - d + 1 + N, & \text{otherwise.} \end{cases}$$

The rows of $\mathbf{X}_{\langle k, d \rangle}$ are enumerated by the d indices $\{i_m, i_{m+1}, \dots, i_k\}$, while its columns are enumerated by the remaining $N - d$ indices. In addition, $\text{fold}_{\langle k, d \rangle}(\mathbf{X}_{\langle k, d \rangle}) = \mathcal{X}$, which represents the inverse process.

Theorem 4.2. Given an N th-order RB tensor $\mathcal{X} \in \mathbb{H}_c^{I_1 \times I_2 \times \dots \times I_N}$ with a RBTR decomposition format $\mathfrak{TR}(\mathcal{Z}_1, \mathcal{Z}_2, \dots, \mathcal{Z}_N)$ and its RBTR rank $\mathbf{r} = [r_1, r_2, \dots, r_N]$,

we have

$$\text{rank}(\mathbf{X}_{\langle k, d \rangle}) \leq r_{k+1} r_m.$$

Proof.

$$\begin{aligned} & \mathbf{X}_{\langle k, d \rangle}(\overline{i_m i_{m+1} \cdots i_k}, \overline{i_{k+1} \cdots i_{m-1}}) \\ &= \mathcal{X}(i_1, i_2, \dots, i_N) \\ &= \text{Tr}\{\mathbf{Z}_1(i_1) \mathbf{Z}_2(i_2) \cdots \mathbf{Z}_N(i_N)\} \\ &= \text{Tr}\{\mathbf{Z}_m(i_m) \cdots \mathbf{Z}_k(i_k) \mathbf{Z}_{k+1}(i_{k+1}) \cdots \mathbf{Z}_{m-1}(i_{m-1})\} \\ &= \text{Tr}\{\mathbf{A}(\overline{i_m i_{m+1} \cdots i_k}) \mathbf{B}(\overline{i_{k+1} \cdots i_{m-1}})\}, \end{aligned}$$

where $\mathcal{A} \in \mathbb{H}_c^{r_m \times I_m I_{m+1} \cdots I_k \times r_{k+1}}$ with

$$\mathbf{A}(\overline{i_m i_{m+1} \cdots i_k}) = \mathbf{Z}_m(i_m) \mathbf{Z}_{m+1}(i_{m+1}) \cdots \mathbf{Z}_k(i_k)$$

and $\mathcal{B} \in \mathbb{R}^{r_{k+1} \times I_{k+1} I_{k+2} \cdots I_{m-1} \times r_m}$ with

$$\mathbf{B}(\overline{i_{k+1} i_{k+2} \cdots i_{m-1}}) = \mathbf{Z}_{k+1}(i_{k+1}) \mathbf{Z}_{k+2}(i_{k+2}) \cdots \mathbf{Z}_{m-1}(i_{m-1}).$$

Then

$$\begin{aligned} & \mathbf{X}_{\langle k, d \rangle}(\overline{i_m i_{m+1} \cdots i_k}, \overline{i_{k+1} \cdots i_{m-1}}) \\ &= \sum_{\gamma_{k+1}=1}^{r_{k+1}} \sum_{\gamma_m=1}^{r_m} \mathcal{A}(\gamma_m, \overline{i_m i_{m+1} \cdots i_k}, \gamma_{k+1}) \mathcal{B}(\gamma_{k+1}, \overline{i_{k+1} \cdots i_{m-1}}, \gamma_m) \\ &= \sum_{\gamma_{k+1} \gamma_m=1}^{r_{k+1} r_m} \mathbf{A}_{(2)}(\overline{i_m i_{m+1} \cdots i_k}, \gamma_{k+1} \gamma_m) \mathbf{B}_{[2]}^T(\gamma_{k+1} \gamma_m, \overline{i_{k+1} \cdots i_{m-1}}). \end{aligned}$$

Based on the above processes, we have $\mathbf{X}_{\langle k, d \rangle} = \mathbf{A}_{(2)} \mathbf{B}_{[2]}^T$. Therefore, by using (f) of Theorem 2.3,

$$\begin{aligned} \text{rank}(\mathbf{X}_{\langle k, d \rangle}) &\leq \min(\text{rank}(\mathbf{A}_{(2)}), \text{rank}(\mathbf{B}_{[2]}^T)) \\ &= \frac{1}{4} \min(\text{rank}((\mathbf{A}_{(2)})^R), \text{rank}((\mathbf{B}_{[2]}^T)^R)), \end{aligned}$$

that is, $\text{rank}(\mathbf{X}_{\langle k, d \rangle}) \leq r_{k+1} r_m$ as desired. \square

Now, we can transform the LRRBTC problem (14) into the following problem

$$\min_{\mathcal{X}} \sum_{k=1}^N \alpha_k \text{rank}(\mathbf{X}_{\langle k, d \rangle}), \quad \text{s.t.} \quad P_{\Omega}(\mathcal{X}) = P_{\Omega}(\mathcal{T}), \quad (15)$$

where $\alpha_k > 0$ is a scalar weight and $\sum_{k=1}^N \alpha_k = 1$.

However, the optimization problem as formulated in (15) is NP-hard [12]. To address this challenge, the researchers recently have turned to alternative strategies. Among these, minimizing the nuclear norm has emerged as a popular choice. The nuclear norm offers a convex relaxation for the non-convex rank minimization problem, providing an effective approximation [15]. Therefore we propose the reduced biquaternion tensor ring nuclear norm.

Definition 4.3. (RBTR Nuclear Norm)

Let $\mathcal{X} \in \mathbb{H}_c^{I_1 \times I_2 \times \dots \times I_N}$ with a RBTR format. We define its RBTR nuclear norm as:

$$\text{NN}_{\text{RBTR}}(\mathcal{X}) = \sum_{k=1}^N \alpha_k \|\mathbf{X}_{\langle k, d \rangle}\|_*, \quad (16)$$

where α_k 's are the same as ones in (15).

In many representative tensor completion methods currently in use, a technique known as key augmentation has been widely adopted. This approach primarily aims to better mine the data's low-rank structures, as it enhances the representational capability and flexibility towards the original tensor [1]. However, a notable downside is that employing tensor augmentation can introduce block artifacts, manifested as visible block-like distortions in the data.

To overcome this challenge and improve the visual quality of the data, the researchers have proposed the incorporation of total variation (TV) regularization [4]. TV regularization is a mathematical technique designed to smooth the values within an image or tensor, while preserving its primary structures and features. The underlying idea is to penalize large local variations within the tensor, promoting data continuity and smoothness. As a result, TV regularization can effectively reduce block artifacts caused by tensor augmentation, thus enhancing the performance and quality of the completion task. The isotropic TV is defined by

$$\text{TV}(\mathcal{X}) = \sum_{m=1}^{I_1} \sum_{n=1}^t \sqrt{|D_{m,n}^1 \mathbf{X}_{(1)}|^2 + |D_{m,n}^2 \mathbf{X}_{(1)}|^2}, \quad (17)$$

where $\mathbf{X}_{(1)} \in \mathbb{H}_c^{I_1 \times t}$, $t = \prod_{i=2}^N I_i$. At the (m, n) -th pixel within the matrix $\mathbf{X}_{(1)}$, $D_{m,n}^1 \mathbf{X}_{(1)}$ represents the gradient in the horizontal axis and $D_{m,n}^2 \mathbf{X}_{(1)}$ represents the gradient in the vertical axis. Correspondingly, the operators $D_{m,n}^1$ and $D_{m,n}^2$ denote the discrete gradients in the horizontal and vertical directions.

By utilizing RBTR nuclear norm and TV regularization, our RBTR-TV method is proposed as:

$$\begin{aligned} \min_{\mathcal{X}} \quad & \sum_{k=1}^N \alpha_k \|\mathbf{X}_{\langle k, d \rangle}\|_* + \lambda \text{TV}(\mathcal{X}) \\ \text{s.t.} \quad & P_{\Omega}(\mathcal{X}) = P_{\Omega}(\mathcal{T}), \end{aligned} \quad (18)$$

where λ is the regularization parameter.

To solve the (18), we first introduce auxiliary reduced biquaternion variables \mathcal{A}_k ($k = 1, 2, \dots, N$) and \mathcal{Z} by using the variable-splitting technique as follows:

$$\begin{aligned} \min_{\mathcal{X}, \mathcal{A}_k, \mathcal{Z}} \quad & \sum_{k=1}^N \alpha_k \|\mathbf{A}_{k \langle k, d \rangle}\|_* + \lambda \sum_{m=1}^{I_1} \sum_{n=1}^t \|\mathbf{E}_{m,n}\|_2 \\ \text{s.t.} \quad & P_{\Omega}(\mathcal{X}) = P_{\Omega}(\mathcal{T}), \\ & \mathcal{X} = \mathcal{A}_k, \mathcal{X} = \mathcal{Z}, \\ & \mathbf{D}_1 \mathbf{Z}_{(1)} = \mathbf{E}_1, \mathbf{D}_2 \mathbf{Z}_{(1)} = \mathbf{E}_2, \end{aligned}$$

where $\mathbf{Z}_{(1)}$ is the classical mode-1 unfolding of \mathcal{Z} , $\mathbf{E}_{m,n} = [(\mathbf{E}_1)_{m,n}, (\mathbf{E}_2)_{m,n}]$ and $\mathbf{E}_1, \mathbf{E}_2$ denote the outcomes of applying horizontal and vertical discrete gradient matrices \mathbf{D}_1 and \mathbf{D}_2 to $\mathbf{Z}_{(1)}$, respectively.

The augmented Lagrangian function is defined using the ADMM framework as follows:

$$\begin{aligned}
& \mathcal{L}(\mathcal{X}, \{\mathcal{A}_k\}_{k=1}^N, \mathcal{Z}, \{\mathbf{E}_i\}_{i=1}^2, \{\mathcal{B}_k\}_{k=1}^N, \mathcal{Q}, \{\mathbf{F}_i\}_{i=1}^2) \\
&= \sum_{k=1}^N \alpha_k \|\mathbf{A}_{k \langle k, d \rangle}\|_* + \lambda \sum_{m=1}^{I_1} \sum_{n=1}^t \|\mathbf{E}_{m,n}\|_2 \\
&+ \sum_{k=1}^N \left(\frac{\beta_1}{2} \|\mathcal{X} - \mathcal{A}_k\|_F^2 + \Re(\langle \mathcal{X} - \mathcal{A}_k, \mathcal{B}_k \rangle) \right) \\
&+ \frac{\beta_2}{2} \|\mathcal{X} - \mathcal{Z}\|_F^2 + \Re(\langle \mathcal{X} - \mathcal{Z}, \mathcal{Q} \rangle) \\
&+ \sum_{i=1}^2 \left(\frac{\beta_3}{2} \|\mathbf{D}_i \mathbf{Z}_{(1)} - \mathbf{E}_i\|_F^2 + \Re(\langle \mathbf{D}_i \mathbf{Z}_{(1)} - \mathbf{E}_i, \mathbf{F}_i \rangle) \right),
\end{aligned}$$

where $\mathcal{B}_k (k = 1, 2, \dots, N)$, \mathcal{Q} and $\mathbf{F}_i (i = 1, 2)$ are Lagrange multipliers, $\beta_i > 0 (i = 1, 2, 3)$ is the penalty parameter, and p represents the number of iterations. Next, we solve the problem using the iterative approach described below:

$$\left\{ \begin{array}{l}
\mathcal{X}^{p+1} = \underset{P_\Omega(\mathcal{X})=P_\Omega(\mathcal{T})}{\operatorname{argmin}} \mathcal{L}(\mathcal{X}, \{\mathcal{A}_k^p\}_{k=1}^N, \mathcal{Z}^p, \{\mathcal{B}_k^p\}_{k=1}^N, \mathcal{Q}^p) \\
\mathcal{A}_k^{p+1} = \underset{\mathcal{A}_k}{\operatorname{argmin}} \mathcal{L}(\mathcal{X}^{p+1}, \mathcal{A}_k, \mathcal{B}_k^p) \\
\mathcal{Z}^{p+1} = \underset{\mathcal{Z}}{\operatorname{argmin}} \mathcal{L}(\mathcal{X}^{p+1}, \mathcal{Z}, \{\mathbf{E}_i^p\}_{i=1}^2, \mathcal{Q}^p, \{\mathbf{F}_i^p\}_{i=1}^2) \\
\mathbf{E}_i^{p+1} = \underset{\mathbf{E}_i}{\operatorname{argmin}} \mathcal{L}(\mathcal{Z}^{p+1}, \mathbf{E}_i, \mathbf{F}_i^p) \\
\mathcal{B}_k^{p+1} = \mathcal{B}_k^p + \beta_1 (\mathcal{X}^{p+1} - \mathcal{A}_k^{p+1}) \\
\mathcal{Q}^{p+1} = \mathcal{Q}^p + \beta_2 (\mathcal{X}^{p+1} - \mathcal{Z}^{p+1}) \\
\mathbf{F}_i^{p+1} = \mathbf{F}_i^p + \beta_3 (\mathbf{D}_i \mathbf{Z}_{(1)}^{p+1} - \mathbf{E}_i^{p+1}).
\end{array} \right.$$

Updating \mathcal{X} :

$$\begin{aligned}
\mathcal{X}^{p+1} &= \underset{P_\Omega(\mathcal{X})=P_\Omega(\mathcal{T})}{\operatorname{argmin}} \mathcal{L}(\mathcal{X}, \{\mathcal{A}_k^p\}_{k=1}^N, \mathcal{Z}^p, \{\mathcal{B}_k^p\}_{k=1}^N, \mathcal{Q}^p) \\
&= \underset{P_\Omega(\mathcal{X})=P_\Omega(\mathcal{T})}{\operatorname{argmin}} \sum_{k=1}^N \left(\frac{\beta_1}{2} \|\mathcal{X} - \mathcal{A}_k^p\|_F^2 + \Re(\langle \mathcal{X} - \mathcal{A}_k^p, \mathcal{B}_k^p \rangle) \right) \\
&\quad + \frac{\beta_2}{2} \|\mathcal{X} - \mathcal{Z}^p\|_F^2 + \Re(\langle \mathcal{X} - \mathcal{Z}^p, \mathcal{Q}^p \rangle).
\end{aligned}$$

For this optimization problem, adding a constant unrelated to \mathcal{X} does not affect the

optimization outcome. Therefore, we transform the problem into:

$$\begin{aligned}
\mathcal{X}^{p+1} &= \operatorname{argmin}_{P_\Omega(\mathcal{X})=P_\Omega(\mathcal{T})} \sum_{k=1}^N \left(\frac{\beta_1}{2} \left(\|\mathcal{X} - \mathcal{A}_k^p\|_F^2 + 2\Re \left(\langle \mathcal{X} - \mathcal{A}_k^p, \frac{\mathcal{B}_k^p}{\beta_1} \rangle \right) + \left\| \frac{\mathcal{B}_k^p}{\beta_1} \right\|_F^2 \right) \right) \\
&\quad + \frac{\beta_2}{2} \left(\|\mathcal{X} - \mathcal{Z}^p\|_F^2 + 2\Re \left(\langle \mathcal{X} - \mathcal{Z}^p, \frac{\mathcal{Q}^p}{\beta_2} \rangle \right) + \frac{\mathcal{Q}^p}{\beta_2} \right) \\
&= \operatorname{argmin}_{P_\Omega(\mathcal{X})=P_\Omega(\mathcal{T})} \sum_{k=1}^N \left(\frac{\beta_1}{2} \left\| \mathcal{X} - \mathcal{A}_k^p + \frac{\mathcal{B}_k^p}{\beta_1} \right\|_F^2 \right) + \frac{\beta_2}{2} \left\| \mathcal{X} - \mathcal{Z}^p + \frac{\mathcal{Q}^p}{\beta_2} \right\|_F^2 \\
&= P_{\Omega^c} \left(\frac{\sum_{k=1}^N (\beta_1 \mathcal{A}_k^p - \mathcal{B}_k^p) + \beta_2 \mathcal{Z}^p - \mathcal{Q}^p}{N\beta_1 + \beta_2} \right) + P_\Omega(\mathcal{T}), \tag{19}
\end{aligned}$$

where Ω^c represents the complement of Ω , which contains all the elements that are not in Ω .

Updating \mathcal{A}_k :

$$\begin{aligned}
\mathcal{A}_k^{p+1} &= \operatorname{argmin}_{\mathcal{A}_k} \mathcal{L}(\mathcal{X}^{p+1}, \mathcal{A}_k, \mathcal{B}_k^p) \\
&= \operatorname{argmin} \alpha_k \|\mathbf{A}_{k<k,d>}\|_* + \frac{\beta_1}{2} \|\mathcal{X}^{p+1} - \mathcal{A}_k\|_F^2 + \Re(\langle \mathcal{X}^{p+1} - \mathcal{A}_k, \mathcal{B}_k^p \rangle) \\
&= \operatorname{argmin} \alpha_k \|\mathbf{A}_{k<k,d>}\|_* + \frac{\beta_1}{2} \left\| \mathcal{X}^{p+1} - \mathcal{A}_k + \frac{\mathcal{B}_k^p}{\beta_1} \right\|_F^2 \\
&= \operatorname{argmin} \alpha_k \|\mathbf{A}_{k<k,d>}\|_* + \frac{\beta_1}{2} \left\| \mathbf{X}_{<k,d>}^{p+1} - \mathbf{A}_{k<k,d>} + \frac{\mathbf{B}_{k<k,d>}^p}{\beta_1} \right\|_F^2.
\end{aligned}$$

Denote $\mathbf{\Gamma} = \mathbf{X}_{<k,d>}^{p+1} + \frac{\mathbf{B}_{k<k,d>}^p}{\beta_1}$ and let $\mathbf{\Gamma} = \mathbf{U}\mathbf{\Sigma}\mathbf{V}^H$, $\tau = \frac{\alpha_k}{\beta_1}$. Thus \mathcal{A}_k^{p+1} has the closed-form solution, which follows a proof process analogous to that in the quaternion domain [2], and it can be presented as:

$$\mathcal{A}_k^{p+1} = \operatorname{fold}_{<k,d>}(\mathbf{U}S_\tau(\mathbf{\Sigma})\mathbf{V}^H), \tag{20}$$

where $S_\tau(\mathbf{\Sigma}) = \operatorname{diag}(\max(0, \sigma_i(\mathbf{\Gamma}) - \tau))$.

Updating \mathcal{Z} :

$$\begin{aligned}
\mathcal{Z}^{p+1} &= \operatorname{argmin}_{\mathcal{Z}} \mathcal{L}(\mathcal{X}^{p+1}, \mathcal{Z}, \{\mathbf{E}_i^p\}_{i=1}^2, \mathcal{Q}^p, \{\mathbf{F}_i^p\}_{i=1}^2) \\
&= \operatorname{argmin} \frac{\beta_2}{2} \|\mathcal{X}^{p+1} - \mathcal{Z}\|_F^2 + \Re(\langle \mathcal{X}^{p+1} - \mathcal{Z}, \mathcal{Q}^p \rangle) \\
&\quad + \sum_{i=1}^2 \left(\frac{\beta_3}{2} \|\mathbf{D}_i \mathbf{Z}_{(1)} - \mathbf{E}_i^p\|_F^2 + \Re(\langle \mathbf{D}_i \mathbf{Z}_{(1)} - \mathbf{E}_i^p, \mathbf{F}_i^p \rangle) \right) \\
&= \operatorname{argmin} \frac{\beta_2}{2} \|\mathcal{X}^{p+1} - \mathcal{Z} + \frac{\mathcal{Q}^p}{\beta_2}\|_F^2 + \sum_{i=1}^2 \left(\frac{\beta_3}{2} \left\| \mathbf{D}_i \mathbf{Z}_{(1)} - \mathbf{E}_i^p + \frac{\mathbf{F}_i^p}{\beta_3} \right\|_F^2 \right).
\end{aligned}$$

Since the tensor's Frobenius norm and the tensor's unfolded matrix's Frobenius norm are the same, the aforementioned problem is transformed into the following

formula:

$$\mathbf{Z}_{(1)}^{p+1} = \operatorname{argmin} \frac{\beta_2}{2} \|\mathbf{X}_{(1)}^{p+1} - \mathbf{Z}_{(1)} + \frac{\mathbf{Q}_{(1)}^p}{\beta_2}\|_F^2 + \sum_{i=1}^2 \left(\frac{\beta_3}{2} \|\mathbf{D}_i \mathbf{Z}_{(1)} - \mathbf{E}_i^p + \frac{\mathbf{F}_i^p}{\beta_3}\|_F^2 \right).$$

The problem can be equivalent to the following formula:

$$\mathbf{A} \mathbf{Z}_{(1)}^{p+1} = \mathbf{B},$$

where

$$\mathbf{A} = \beta_2 \mathbf{I} + \beta_3 (\mathbf{D}_1^T \mathbf{D}_1 + \mathbf{D}_2^T \mathbf{D}_2), \quad \mathbf{B} = \beta_2 \mathbf{X}_{(1)}^{p+1} + \mathbf{Q}_{(1)}^p + \beta_3 \mathbf{D}_1^T \mathbf{E}_1^p - \mathbf{D}_1^T \mathbf{F}_1^p + \beta_3 \mathbf{D}_2^T \mathbf{E}_2^p - \mathbf{D}_2^T \mathbf{F}_2^p.$$

As demonstrated in [20], while the spatial domain convolution of two quaternion matrices cannot be computed through the multiplication of their Fourier transforms in the frequency domain, the convolution operation for RB matrices in the spatial domain does equate to their multiplication in the frequency domain, which is similar to the properties of convolution for real-valued matrices. Therefore the problem can be solved quickly by using the Fourier transform [4]:

$$\mathbf{Z}_{(1)}^{p+1} = \mathcal{F}^{-1} \left(\frac{\mathcal{F}(\mathbf{B})}{\mathcal{F}(\mathbf{A})} \right). \quad (21)$$

Updating \mathbf{E}_i :

$$\begin{aligned} \mathbf{E}_i^{p+1} &= \operatorname{argmin}_{\mathbf{E}_i} \mathcal{L}(\mathbf{Z}^{p+1}, \mathbf{E}_i, \mathbf{F}_i^p) \\ &= \operatorname{argmin}_{\mathbf{E}_i} \lambda \sum_{m=1}^{I_1} \sum_{n=1}^t \|\mathbf{E}_{m,n}\|_2 + \sum_{i=1}^2 \left(\frac{\beta_3}{2} \|\mathbf{D}_i \mathbf{Z}_{(1)}^{p+1} - \mathbf{E}_i\|_F^2 + \Re(\langle \mathbf{D}_i \mathbf{Z}_{(1)}^{p+1} - \mathbf{E}_i, \mathbf{F}_i^p \rangle) \right) \\ &= \operatorname{argmin}_{\mathbf{E}_i} \lambda \sum_{m=1}^{I_1} \sum_{n=1}^t \|\mathbf{E}_{m,n}\|_2 + \sum_{i=1}^2 \left(\frac{\beta_3}{2} \|\mathbf{D}_i \mathbf{Z}_{(1)}^{p+1} - \mathbf{E}_i + \frac{\mathbf{F}_i^p}{\beta_3}\|_F^2 \right). \end{aligned}$$

In order to find the optimal \mathbf{E}_i , one must solve I_t independent minimization problems as follows due to the objective function being the sum of squared terms of each element in \mathbf{E}_i , which are independent of one another:

$$\operatorname{argmin}_{(\mathbf{E}_1, \mathbf{E}_2)_{m,n}} \lambda \sqrt{|(\mathbf{E}_1)_{m,n}|^2 + |(\mathbf{E}_2)_{m,n}|^2} + \frac{\beta_3}{2} \sum_{i=1}^2 \left| (\mathbf{D}_i \mathbf{Z}_{(1)}^{p+1})_{m,n} - (\mathbf{E}_i)_{m,n} + \frac{(\mathbf{F}_i^p)_{m,n}}{\beta_3} \right|^2.$$

As proven in Theorem 2.5, we have:

$$[(\mathbf{E}_1)_{m,n}, (\mathbf{E}_2)_{m,n}] = \max \left\{ \|\mathbf{w}_{m,n}\|_2 - \frac{\lambda}{\beta_3}, 0 \right\} \frac{\mathbf{w}_{m,n}}{\|\mathbf{w}_{m,n}\|_2}, \quad (22)$$

where

$$\mathbf{w}_{m,n} = \left[(\mathbf{D}_1 \mathbf{Z}_{(1)}^{p+1})_{m,n} + \frac{(\mathbf{F}_1^p)_{m,n}}{\beta_3}, (\mathbf{D}_2 \mathbf{Z}_{(1)}^{p+1})_{m,n} + \frac{(\mathbf{F}_2^p)_{m,n}}{\beta_3} \right] \quad (1 \leq m \leq I_1, 1 \leq n \leq t).$$

Updating $\mathcal{B}_k, \mathcal{Q}, \mathbf{F}_i$:

$$\mathcal{B}_k^{p+1} = \mathcal{B}_k^p + \beta_1 (\mathcal{X}^{p+1} - \mathcal{A}_k^{p+1}), \quad (23)$$

$$\mathcal{Q}^{p+1} = \mathcal{Q}^p + \beta_2 (\mathcal{X}^{p+1} - \mathcal{Z}^{p+1}), \quad (24)$$

$$\mathbf{F}_i^{p+1} = \mathbf{F}_i^p + \beta_3 (\mathbf{D}_i \mathbf{Z}_{(1)}^{p+1} - \mathbf{E}_i^{p+1}). \quad (25)$$

Ultimately, we design the following **Algorithm 2** which is a summary of the low-rank RB tensor completion approach, leveraging the RB tensor ring decomposition and the total variation regularization.

Algorithm 2 RBTR-TV

Input: The observed RB tensor $\mathcal{T} \in \mathbb{H}_c^{I_1 \times I_2 \times \dots \times I_N}$, the index set Ω , the parameters: α_k for $k = 1, 2, \dots, N$, the regularization parameters: $\lambda, \beta_1, \beta_2, \beta_3$, and the maximum number of iterations: $maxIter$.

Output: The recovered RB tensor \mathcal{X}^p .

- 1: Initialize: $\{\mathcal{A}_k^0\}_{k=1}^N, \{\mathcal{B}_k^0\}_{k=1}^N, \mathcal{Z}^0, \{\mathbf{E}_i^0\}_{i=1}^2, \mathcal{Q}^0, \{\mathbf{F}_i^0\}_{i=1}^2, p = 0$
 - 2: **while** $\left(\frac{\|\mathcal{X}^{p+1} - \mathcal{X}^p\|_F}{\|\mathcal{X}^p\|_F} > 10^{-5}\right)$ or $(p < maxIter)$ **do**
 - 3: Update \mathcal{X}^{p+1} by using (19)
 - 4: **for** $k = 1$ to N **do**
 - 5: Update \mathcal{A}_k^{p+1} by using (20)
 - 6: **end for**
 - 7: Update \mathcal{Z}^{p+1} by using (21)
 - 8: Update \mathbf{E}_i^{p+1} by using (22)
 - 9: **for** $k = 1$ to N **do**
 - 10: Update \mathcal{B}_k^{p+1} by using (23)
 - 11: **end for**
 - 12: Update \mathcal{Q}^{p+1} by using (24)
 - 13: Update \mathbf{F}_i^{p+1} by using (25)
 - 14: Increment p : $p \leftarrow p + 1$
 - 15: **end while**
-

5 Experiment

5.1 Color image completion

In this section, we compare our proposed RBTR-TV with six baselines in color image completion experiments, including SiLRTC-TT[1], LRQC[3], MF-TTTV[4], TVTRC[9], RTRC[13], and QTT-SRTD[18]. All methods tune parameters according to literature references.

In order to quantitatively compare the completion performance, we use PSNR (see (13)), RSE (see (12)) and Time (in seconds) as metrics. Ten color images, each represented as a $256 \times 256 \times 3$ real tensor, are used to compare RBTR-TV with other methods. In addition, we use ket augmentation technology and change each image into a $4 \times 4 \times 4 \times 4 \times 4 \times 4 \times 4 \times 4 \times 3$ high-order real tensor. After converting to RBs representation, the dimension is $4 \times 4 \times 4 \times 4 \times 4 \times 4 \times 4 \times 4$. We set $\alpha_k = 0.125, \lambda = 0.3, \beta_1 = 5 \times 10^{-3}, \beta_2 = 0.1$, and $\beta_3 = 5 \times 10^{-3}$.

Table 2 shows the performance comparison results at sampling rates SR=5%, 10%, 15%, 20%. The method RBTR-TV consistently outperforms other comparative methods both in PSNR and RSE across all sampling rates. These results indicate the robustness and effectiveness of RBTR-TV in handling various levels of data sparsity. Figure 1 is the visual content based on $SR = 20\%$.

Image	SR Method	5%			10%			15%			20%		
		PSNR	RSE	Time	PSNR	RSE	Time	PSNR	RSE	Time	PSNR	RSE	Time
Airplane	SiLRTC-TT	18.28	0.1697	10.63	19.79	0.1437	15.29	20.97	0.1260	13.71	22.03	0.1120	11.31
	RTRC	16.33	0.2145	29.61	20.35	0.1369	30.57	21.92	0.1139	24.58	23.73	0.0933	28.48
	MF-TTTV	20.06	0.1350	362.91	22.67	0.1000	345.75	24.25	0.0834	253.74	25.44	0.0727	189.10
	TVTRC	10.98	0.3841	36.71	12.73	0.3139	37.06	16.65	0.2001	38.29	20.01	0.1358	27.20
	LRQC	16.84	0.1957	7.55	21.05	0.1206	7.53	22.70	0.0996	5.54	23.94	0.0864	4.61
	QTT-SRTD	19.82	0.1355	46.06	21.50	0.1106	44.19	23.07	0.0948	45.14	24.26	0.0791	41.29
	RBTR-TV	22.05	0.1113	12.91	24.04	0.0900	11.43	25.40	0.0756	11.80	26.78	0.0645	11.17
Peppers	SiLRTC-TT	15.44	0.3408	15.21	18.97	0.2249	15.39	20.57	0.1868	14.06	21.81	0.1623	11.39
	RTRC	12.88	0.4677	29.28	18.39	0.2478	28.19	21.42	0.1716	29.33	22.43	0.1523	29.89
	MF-TTTV	18.63	0.2309	347.56	22.86	0.1419	368.07	24.77	0.1139	347.05	26.17	0.0969	286.79
	TVTRC	9.34	0.6733	36.34	14.30	0.3804	37.00	17.66	0.2582	34.80	18.77	0.2273	24.75
	LRQC	15.96	0.3140	6.35	19.51	0.2087	6.68	22.60	0.1687	5.23	24.04	0.1422	5.21
	QTT-SRTD	20.79	0.1748	54.38	22.97	0.1341	53.10	24.74	0.1148	57.66	25.83	0.0991	50.92
	RBTR-TV	22.91	0.1440	11.50	25.16	0.1089	11.40	26.88	0.0905	11.45	28.30	0.0774	11.58
Baboon	SiLRTC-TT	15.71	0.3045	16.49	17.58	0.2456	16.04	18.66	0.2163	15.10	19.39	0.1989	12.50
	RTRC	13.02	0.4153	27.62	17.80	0.2589	28.21	19.60	0.1980	25.75	20.43	0.1852	33.09
	MF-TTTV	16.36	0.2809	408.78	18.71	0.2141	349.43	19.86	0.1876	361.14	20.72	0.1700	259.97
	TVTRC	10.84	0.5298	36.44	13.40	0.3946	36.37	16.24	0.2846	38.19	18.25	0.2258	41.30
	LRQC	16.21	0.2857	6.77	17.97	0.2332	5.88	19.10	0.2048	5.01	19.99	0.1849	4.35
	QTT-SRTD	18.42	0.2178	57.46	19.65	0.1878	56.35	20.90	0.1647	61.12	21.73	0.1260	54.67
	RBTR-TV	19.97	0.1868	12.42	21.33	0.1596	13.49	22.39	0.1415	12.03	23.44	0.1253	13.13
Female	SiLRTC-TT	19.43	0.3574	15.78	22.05	0.2617	14.69	23.63	0.2172	11.29	24.96	0.1855	9.86
	RTRC	16.79	0.4842	19.13	23.25	0.2284	19.09	25.33	0.1789	19.74	26.35	0.1586	19.21
	MF-TTTV	21.80	0.2853	350.61	26.50	0.1661	345.74	28.27	0.1355	266.60	29.86	0.1129	244.84
	TVTRC	13.02	0.7846	12.38	18.24	0.4301	40.62	20.76	0.3215	37.36	22.95	0.2502	22.32
	LRQC	15.90	0.5627	6.38	22.54	0.2620	7.06	25.66	0.1830	6.09	27.48	0.1485	5.50
	QTT-SRTD	24.22	0.1917	71.04	26.17	0.1509	70.10	27.61	0.1267	75.67	28.75	0.1104	75.32
	RBTR-TV	26.35	0.1691	12.27	28.67	0.1294	11.43	30.31	0.1071	11.51	31.69	0.0915	11.57
House1	SiLRTC-TT	16.70	0.2120	14.26	18.83	0.1656	15.35	20.33	0.1393	14.25	21.60	0.1203	11.32
	RTRC	14.36	0.2785	20.06	18.04	0.1921	29.13	20.46	0.1396	26.10	22.48	0.1118	27.28
	MF-TTTV	19.92	0.1566	344.68	23.07	0.1090	344.32	24.65	0.0909	291.64	26.03	0.0775	208.95
	TVTRC	11.13	0.4311	39.24	16.78	0.2249	36.47	18.12	0.1927	40.02	20.55	0.1457	23.73
	LRQC	17.65	0.2034	6.59	21.46	0.1311	7.57	23.01	0.1097	5.65	24.32	0.0943	4.45
	QTT-SRTD	20.53	0.1418	47.91	22.52	0.1114	47.89	23.49	0.0932	47.89	25.31	0.0795	46.63
	RBTR-TV	21.95	0.1240	11.42	23.98	0.0981	11.44	25.54	0.0820	11.36	26.86	0.0705	11.22
Tree	SiLRTC-TT	16.34	0.2671	16.51	18.69	0.2053	15.41	20.14	0.1750	14.24	21.33	0.1528	11.52
	RTRC	13.44	0.3790	29.80	19.59	0.1892	21.83	21.14	0.1562	29.22	22.65	0.1322	27.37
	MF-TTTV	18.16	0.2243	344.49	22.61	0.1344	383.65	24.24	0.1114	344.23	25.85	0.0925	296.94
	TVTRC	10.80	0.5234	36.21	13.94	0.3649	37.16	18.63	0.2127	40.96	19.80	0.1857	16.23
	LRQC	16.59	0.2687	6.55	20.19	0.1776	5.76	22.27	0.1397	4.97	23.46	0.1219	4.22
	QTT-SRTD	19.84	0.1805	53.72	21.74	0.1417	50.23	23.40	0.1152	50.23	24.61	0.1000	54.27
	RBTR-TV	21.42	0.1541	11.49	23.67	0.1189	13.70	25.50	0.0964	11.52	26.75	0.0834	11.58
Butterfly	SiLRTC-TT	13.72	0.3984	15.07	15.83	0.3103	15.14	17.57	0.2534	15.93	18.99	0.2158	13.97
	RTRC	12.41	0.4771	22.32	16.07	0.3158	38.72	18.83	0.2227	27.50	20.49	0.1885	20.09
	MF-TTTV	16.98	0.2735	362.65	20.42	0.1841	362.66	21.93	0.1491	369.05	24.15	0.1223	249.03
	TVTRC	7.83	0.7840	38.53	9.23	0.6672	38.11	12.82	0.4413	38.29	14.59	0.3602	16.72
	LRQC	16.55	0.3392	7.29	18.98	0.2505	5.22	20.85	0.2046	4.33	21.99	0.1736	3.86
	QTT-SRTD	17.01	0.2702	59.37	19.27	0.2048	59.41	21.06	0.1568	57.78	22.57	0.1370	57.70
	RBTR-TV	18.50	0.2288	12.35	21.21	0.1669	13.12	22.75	0.1397	12.91	24.47	0.1145	13.16
House2	SiLRTC-TT	19.11	0.1766	16.51	21.52	0.1347	15.48	23.19	0.1109	12.90	24.42	0.0962	10.48
	RTRC	15.63	0.2703	22.28	22.20	0.1260	22.60	24.11	0.0999	22.58	26.30	0.0773	27.24
	MF-TTTV	24.38	0.1021	342.00	26.32	0.0772	307.20	27.36	0.0657	171.98	29.56	0.0551	130.78
	TVTRC	12.87	0.3865	40.20	16.50	0.2544	43.21	19.62	0.1778	44.91	20.08	0.1686	42.19
	LRQC	19.62	0.1896	5.73	24.40	0.1104	6.07	26.57	0.0869	5.54	27.55	0.0764	4.56
	QTT-SRTD	22.90	0.1120	50.45	25.24	0.0835	53.58	26.90	0.0695	49.67	28.23	0.0593	46.26
	RBTR-TV	24.64	0.0954	12.63	26.84	0.0742	12.92	28.54	0.0613	12.89	29.90	0.0525	12.76
Baby	SiLRTC-TT	19.02	0.1877	14.76	22.34	0.1279	14.91	24.06	0.1041	13.73	25.42	0.0890	10.50
	RTRC	13.94	0.3310	24.80	23.82	0.1075	19.58	25.40	0.0888	19.03	27.31	0.0712	21.43
	MF-TTTV	23.64	0.1169	344.60	26.12	0.0788	248.00	28.94	0.0608	174.40	29.86	0.0546	135.17
	TVTRC	12.15	0.4011	43.30	18.17	0.2007	46.31	21.35	0.1391	21.78	22.70	0.1191	15.36
	LRQC	18.21	0.2445	6.33	24.00	0.1144	6.82	26.84	0.0802	5.83	28.90	0.0634	4.69
	QTT-SRTD	23.47	0.1095	48.10	25.68	0.0828	47.04	27.04	0.0713	44.08	28.10	0.0623	45.23
	RBTR-TV	25.01	0.0928	13.71	27.35	0.0701	12.60	29.29	0.0561	12.35	30.75	0.0474	13.60
Bird	SiLRTC-TT	17.34	0.3849	14.82	19.80	0.2901	15.19	21.91	0.2271	12.58	23.34	0.1929	10.19
	RTRC	14.48	0.5543	23.29	19.21	0.3204	20.28	22.96	0.2111	29.95	24.02	0.1825	27.89
	MF-TTTV	20.35	0.2795	339.42	25.19	0.1582	260.60	28.76	0.1029	244.13	28.81	0.0965	126.61
	TVTRC	12.13	0.7051	39.97	15.30	0.4896	40.87	18.49	0.3389	49.88	20.21	0.2781	23.45
	LRQC	15.85	0.4842	6.95	21.45	0.2674	7.26	24.85	0.1976	5.77	25.91	0.1599	4.72
	QTT-SRTD	23.34	0.1836	64.26	26.23	0.1294	62.94	28.36	0.1044	61.37	29.85	0.0835	63.41
	RBTR-TV	24.98	0.1591	12.81	27.95	0.1129	13.07	30.15	0.0876	12.67	31.83	0.0722	12.64

Table 2: PSNR, RSE and Time of various methods with four sampling rates (bold indicates best performance)



Figure 1: Recovery performance of different methods at SR=20%

5.2 Color video completion

In this experiment, we select four videos² for testing: *bus*, *foreman*, *mother*, and *hall* with SR=10% and SR=20%. Each video was sampled for 15 frames with a size of 256×256 . The methods we compared include SiLRTC-TT[1], MF-TTTV[4], TVTRC[9], RTRC[13], QTT-SRTD[18], and our proposed RBTR-TV.

Table 3 presents the average PSNR, RSE, and Time (in seconds) over all frames for each method. Our proposed RBTR-TV method achieves the best PSNR and RSE values among all the compared methods. Although it is not the fastest in terms of running time, it significantly improves the recovered quality compared to the fastest method. Figure 2 shows the recovery results of frame 1 and frame 15 for the *foreman* and *bus* videos at SR=10%. It can be seen that our proposed method performs better in recovering missing data, especially when a large amount of information is missing.

Video	SR	10%			20%		
		Method	PSNR	RSE	Time	PSNR	RSE
Bus	SiLRTC-TT	18.95	0.3383	4.28	21.62	0.2515	4.57
	RTRC	20.91	0.26083	69.13	23.62	0.2038	62.56
	MF-TTTV	21.33	0.2683	81.08	23.55	0.2049	56.07
	TVTRC	23.03	0.2440	97.44	23.74	0.2185	57.54
	QTT-SRTD	23.76	0.1876	23.73	27.52	0.1349	23.72
	RBTR-TV	25.17	0.1692	18.17	28.31	0.1156	18.27
Foreman	SiLRTC-TT	20.37	0.14407	4.19	25.14	0.0840	4.20
	RTRC	25.29	0.0848	64.41	29.75	0.0512	70.57
	MF-TTTV	25.45	0.0803	67.54	27.82	0.0612	39.53
	TVTRC	26.51	0.08151	35.87	28.67	0.0594	26.32
	QTT-SRTD	27.85	0.0506	23.95	31.13	0.0343	23.68
	RBTR-TV	33.53	0.0318	19.86	36.70	0.0220	19.38
Mother	SiLRTC-TT	25.84	0.0895	4.06	29.58	0.0579	4.93
	RTRC	27.61	0.0738	61.25	32.51	0.0415	60.44
	MF-TTTV	28.18	0.0682	66.91	30.68	0.0511	39.59
	TVTRC	33.32	0.0384	61.74	32.49	0.0417	13.00
	QTT-SRTD	32.03	0.0344	25.32	35.28	0.0230	25.01
	RBTR-TV	38.38	0.0211	18.66	42.11	0.0136	18.50
Hall	SiLRTC-TT	21.94	0.1438	4.06	26.38	0.0873	4.27
	RTRC	26.86	0.0874	61.93	30.59	0.0539	71.81
	MF-TTTV	26.06	0.0883	71.19	29.27	0.0616	41.45
	TVTRC	31.26	0.0528	27.01	32.22	0.0474	11.01
	QTT-SRTD	32.68	0.0336	23.57	36.19	0.0219	23.46
	RBTR-TV	37.79	0.0238	19.34	40.30	0.0171	19.02

Table 3: PSNR, RSE and Time of various methods with two sampling rates (bold indicates best performance)

6 Conclusion and future works

In this work, we propose the reduced biquaternion tensor ring (RBTR) decomposition and present its corresponding algorithm, which reduces storage costs compared to TR-SVD while preserving reconstruction quality. Building on the RBTR decomposition, we further introduce RBTR-TV, a novel low-rank tensor completion

²<http://trace.eas.asu.edu/yuv/>

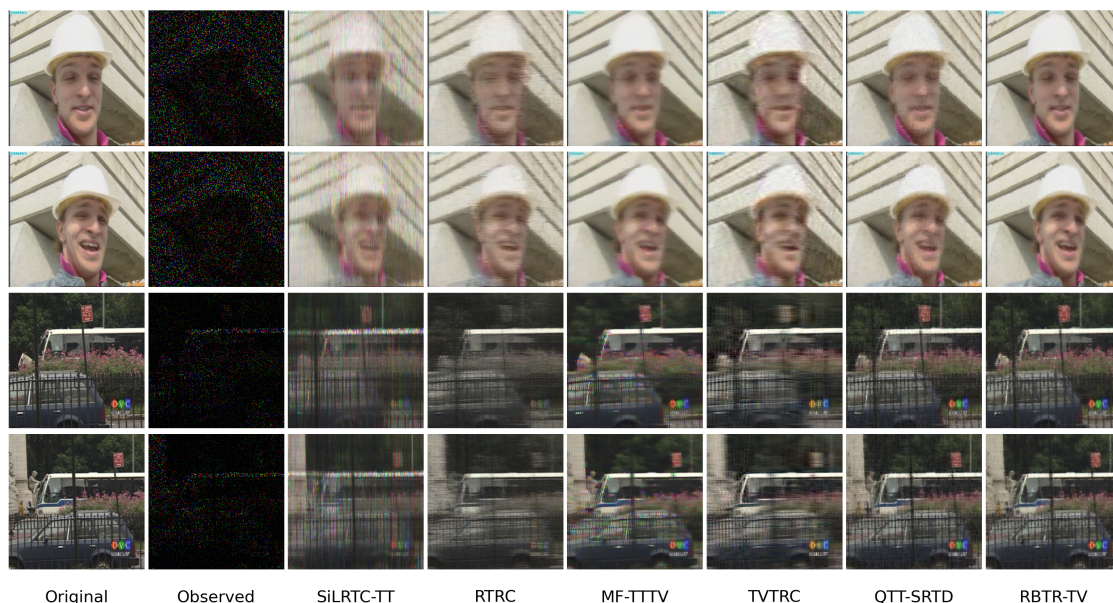


Figure 2: Recovery performance of different methods at SR=10%

method that integrates RBTR rank with total variation (TV) regularization. Experimental results demonstrate its effectiveness in completing color images and videos.

Although RBTR-TV has shown strong performance in color image and video completion, there still remain some challenges. For example, the convergence speed of our current algorithm requires improvement. Our future work will focus on strengthening the theoretical foundation and enhancing the algorithm’s efficiency and speed.

Acknowledgement: This research is partially supported by the National Natural Science Foundation of China (12371023, 12271338), and Canada NSERC, The joint research and Development fund of Wuyi University, Hong Kong and Macao (2019WGALH20).

7 Declarations

Conflict of Interest: The authors have not disclosed any competing interests.

Data Availability Statement: The data supporting the findings of this study are not publicly available due to privacy or ethical restrictions. However, interested researchers may request access to the data by contacting the corresponding author and completing any necessary data sharing agreements.

References

- [1] J.A. Bengua, H.N. Phien, H.D. Tuan, and M.N. Do. Efficient tensor completion for color image and video recovery: Low-rank tensor train. *IEEE Transactions on Image Processing*, 26(5):2466–2479, 2017.
- [2] Y. Chen, X. Xiao, and Y. Zhou. Low-rank quaternion approximation for color image processing. *IEEE Transactions on Image Processing*, 29:1426–1439, 2019.

- [3] J.F. Chen, Q.W. Wang, G.J. Song, and T. Li. Quaternion matrix factorization for low-rank quaternion matrix completion. *Mathematics*, 11(9):2144, 2023.
- [4] M. Ding, T.Z. Huang, T.Y. Ji, X.L. Zhao, and J.H. Yang. Low-rank tensor completion using matrix factorization based on tensor train rank and total variation. *Journal of Scientific Computing*, 81:941–964, 2019.
- [5] W. Ding, Y. Li, and D. Wang. Special least squares solutions of the reduced biquaternion matrix equation $AX = B$ with applications. *Computational and Applied Mathematics*, 40(279), 2021.
- [6] M.T. El-Melegy and A.T. Kamal. Color image processing using reduced biquaternions with application to face recognition in a PCA framework. *Proceedings of the IEEE International Conference on Computer Vision Workshops*, 3039–3046, 2017.
- [7] H. Fanaee-T and J. Gama. Tensor-based anomaly detection: An interdisciplinary survey. *Knowledge-Based Systems*, 98:130–147, 2016.
- [8] S. Gai and X. Huang. Reduced biquaternion convolutional neural network for color image processing. *IEEE Transactions on Circuits and Systems for Video Technology*, 32(3):1061–1075, 2021.
- [9] W. He, L. Yuan, and N. Yokoya. Total-variation-regularized tensor ring completion for remote sensing image reconstruction. In *IEEE International Conference on Acoustics, Speech and Signal Processing (ICASSP)*, 8603–8607, 2019.
- [10] W. He, Y. Chen, N. Yokoya, C. Li, and Q. Zhao. Hyperspectral super-resolution via coupled tensor ring factorization. *Pattern Recognition*, 122:108280, 2022.
- [11] Z.H. He, X.X. Wang, and Y.F. Zhao. Eigenvalues of quaternion tensors with applications to color video processing. *Journal of Scientific Computing*, 94(1):1, 2023.
- [12] C.J. Hillar and L.H. Lim. Most tensor problems are NP-hard. *Journal of the ACM*, 60(6):1–39, 2013.
- [13] H. Huang, Y. Liu, Z. Long, and C. Zhu. Robust low-rank tensor ring completion. *IEEE Transactions on Computational Imaging*, 6:1117–1126, 2020.
- [14] Z. Jia, Q. Jin, M.K. Ng, and X.L. Zhao. Non-local robust quaternion matrix completion for large-scale color image and video inpainting. *IEEE Transactions on Image Processing*, 31:3868–3883, 2022.
- [15] Z. Jia, M.K. Ng, and G.J. Song. Robust quaternion matrix completion with applications to image inpainting. *Numerical Linear Algebra with Applications*, 26(4):e2245, 2019.
- [16] T.G. Kolda and B.W. Bader. Tensor decompositions and applications. *SIAM Review*, 51(3):455–500, 2009.
- [17] X. Liu and Y. Zhang. *Matrices over quaternion algebras. Matrix and Operator Equations and Applications*, Springer, pages 120–185, 2023.
- [18] J. Miao, K.I. Kou, L. Yang, and D. Cheng. Quaternion tensor train rank minimization with sparse regularization in a transformed domain for quaternion tensor completion. *Knowledge-Based Systems*, 284:111222, 2024.

- [19] S.C. Pei, J.H. Chang, J.J. Ding, and M.Y. Chen. Eigenvalues and singular value decompositions of reduced biquaternion matrices. *IEEE Transactions on Circuits and Systems I: Regular Papers*, 55(9):2673–2685, 2008.
- [20] S.C. Pei, J.H. Chang, and J.J. Ding. Commutative reduced biquaternions and their Fourier transform for signal and image processing applications. *IEEE Transactions on Signal Processing*, 52(7):2012–2031, 2004.
- [21] H.D. Schutte and J. Wenzel. Hypercomplex numbers in digital signal processing. In *1990 IEEE International Symposium on Circuits and Systems (ISCAS)*, 2:1557–1560, 1990.
- [22] C. Segre. The real representations of complex elements and extension to bicomplex systems, *Math. Ann.*, 40:413-467, 1892.
- [23] P. Shao, D. Zhang, G. Yang, J. Tao, F. Che, and T. Liu. Tucker decomposition-based temporal knowledge graph completion. *Knowledge-Based Systems*, 238:107841, 2022.
- [24] P.L. Wu, X.L. Zhao, M. Ding, Y.B. Zheng, and L.B. Cui. Tensor ring decomposition-based model with interpretable gradient factors regularization for tensor completion. *Knowledge-Based Systems*, 259:110094, 2023.
- [25] J. Yu, C. Li, Q. Zhao, and G. Zhao. Tensor-ring nuclear norm minimization and application for visual data completion. *IEEE International Conference on Acoustics, Speech and Signal Processing*, 3142–3146, 2019.
- [26] Q. Zhao, G. Zhou, S. Xie, L. Zhang, and A. Cichocki. Tensor ring decomposition. *arXiv preprint arXiv:1606.05535*, 2016.